metabolites

MDPI

Article

Metabolomes and Lipidomes of the Infective Stages of the Gastrointestinal nematodes, *Nippostrongylus brasiliensis* and *Trichuris muris*

Karma Yeshi [1,*], Darren J. Creek [2], Dovile Anderson [2], Edita Ritmejerytė [1], Luke Becker [1], Alex Loukas [1,†] and Phurpa Wangchuk [1,*,†]

1 Centre for Molecular Therapeutics, Australian Institute of Tropical Health and Medicine, James Cook University, Building E4, McGregor Rd, Smithfield, Cairns, QLD 4878, Australia; edita.ritmejeryte@jcu.edu.au (E.R.); luke.becker@jcu.edu.au (L.B.); alex.loukas@jcu.edu.au (A.L.)

2 Drug Delivery, Disposition and Dynamics, Monash Institute of Pharmaceutical Sciences, Monash University, 381 Royal Parade, Parkville, VIC 3052, Australia; darren.creek@monash.edu (D.J.C.); dovile.anderson@monash.edu (D.A.)

* Correspondence: karma.yeshi@my.jcu.edu.au (K.Y.); phurpa.wangchuk@jcu.edu.au (P.W.)

† Equally contributed as senior authors.

Received: 23 October 2020; Accepted: 3 November 2020; Published: 6 November 2020

Abstract: Soil-transmitted helminths, including hookworms and whipworms, infect billions of people worldwide. Their capacity to penetrate and migrate through their hosts' tissues is influenced by the suite of molecules produced by the infective developmental stages. To facilitate a better understanding of the immunobiology and pathogenicity of human hookworms and whipworms, we investigated the metabolomes of the infective stage of *Nippostrongylus brasiliensis* third-stage larvae (L3) which penetrate the skin and *Trichuris muris* eggs which are orally ingested, using untargeted liquid chromatography–mass spectrometry (LC-MS). We identified 55 polar metabolites through Metabolomics Standard Initiative level-1 (MSI-I) identification from *N. brasiliensis* and *T. muris* infective stages, out of which seven were unique to excretory/secretory products (ESPs) of *N. brasiliensis* L3. Amino acids were a principal constituent (33 amino acids). Additionally, we identified 350 putative lipids, out of which 28 (all known lipids) were unique to N. brasiliensis L3 somatic extract and four to *T. muris* embryonated egg somatic extract. Glycerophospholipids and glycerolipids were the major lipid groups. The catalogue of metabolites identified in this study shed light on the biology, and possible therapeutic and diagnostic targets for the treatment of these critical infectious pathogens. Moreover, with the growing body of literature on the therapeutic utility of helminth ESPs for treating inflammatory diseases, a role for metabolites is likely but has received little attention thus far.

Keywords: metabolites; infective stage; *Nippostrongylus brasiliensis*; *Trichuris muris*; parasites; LC-MS; metabolomic; lipidomic

1. Introduction

Infection with parasitic helminths is one of the most common and detrimental of the neglected tropical diseases [1]. Indeed, eight out of the 17 recognised neglected tropical diseases are caused by parasitic helminths [2]. More than 1.5 billion people (approximately 24% of the world's population) are infected with soil-transmitted helminth infections (STHIs) [3] and contribute to a substantial burden of human disease and disability worldwide. The roundworm (*Ascaris lumbricoides*), the whipworm (*Trichuris trichiura*), and hookworms (*Necator americanus* and *Ancylostoma duodenale*) are the major Soil-transmitted helminths (STHs) that infect humans. Unlike *T. trichiura* and *A. lumbricoides*, which are prevalent among young children, *N. americanus* and *A. duodenale* tend to infect older

children and adults [4,5]. Soil-transmitted helminths are ubiquitous in tropical climates and rural temperate areas with inadequate sanitation facilities—that is, mostly poverty-stricken areas across the world. There is no vaccine for any human helminth infections, and current control efforts focus on mass drug administration, which is only partially effective [6]. Currently, the World Health Organization recommends that anthelmintic drugs such as mebendazole and albendazole are commonly used for mass administration to control STHIs [7], but they do not give lasting protection against re-infection. Meanwhile, other treatment drugs such as niclosamide (for *Taenia saginata*), piperazine (for *A. lumbricoides*), and ivermectin (for *Strongyloides stercoralis*) [8] are not suitable for mass control.

Eradication of helminths is challenging, mainly due to their complex life-cycles. Hookworms enter the human hosts when their infective stage 3 larvae (L3) penetrate the skin. Initially, L3 migrates through subcutaneous venules and lymphatics and then subsequently enters the afferent circulation to reach inside the lungs [4]. From there, L3 break through the alveolar spaces and are coughed up and swallowed into the gastrointestinal tract as they mature into L4 and adulthood. Maturation proceeds in the small intestine, where L3 moult twice to become adult male and female hookworms. After mating, female worms produce thousands of eggs that exit the body in the faeces. Whipworms, on the other hand, enter the human host through the ingestion of embryonated eggs from the environment. First-stage (L1) larvae hatch from the eggs and penetrate the epithelial cells at the crypt base to undertake an intracellular existence, where larvae grow and moult through the larval (L2, L3 and L4) and adult stages [9]. Examining helminth eggs in stool samples by Kato-Katz thick-smear technique is the only widely used diagnostic tool in helminth epidemiology [10,11], but this technique is less sensitive in the case of low-intensity helminth infections. Alternative sensitive diagnostic tools such as FLOTAC (a multivalent faecal egg count technique) and McMaster are available [7,12], but they are not adequate. It is, therefore, essential to understand these helminths holistically and devise precise diagnostic tools and effective treatment regimens that would provide long-term protection against diseases caused by STHs.

While there are numerous published studies on STH genomes [13–17] and proteomes [18–20], less attention has been afforded to their metabolomes [21,22] and, specifically, the lipidome [23]. A number of studies [24,25] have shown the importance of STH excretory/secretory products (ESPs) in host–parasite communication, including parasite survival and host protection against immunopathology. For example, ESPs such as TT47 and TM43 produced by whipworms are important for invasion of the gut wall by forming a pore in the epithelial cell membrane [26], and the major ESP, p43m, suppresses secretion of IL-13, a cytokine with anti-helminth properties [27]. Adult *Necator* and *Ancylostoma* hookworms release proteases [28] and anti-coagulant peptides [29] into the infection site to digest the host's mucosal tissues and secrete abundant netrin-like proteins to suppress inflammatory responses by inducing regulatory T cells [30]. Moreover, a small-molecule linoleic acid, used by the cercariae of *Schistosoma mansoni* to produce prostaglandin, PGE2, helps them to successfully migrate inside their host [31]. However, very little is known about the small-molecule complement of STHs, particularly of their infective stages.

Since it is challenging to obtain parasite material from humans, in this study, we used the rodent model STH parasites, *N. brasiliensis* (model organism for the human hookworms *Ancylostoma* and *Necator* spp.) and *T. muris* (model organism for whipworm *T. trichiura*) to characterise and identify small-molecule components of their infective stages. Previously, we reported the ESP metabolomes of their adult developmental stages, both of which reside in the gut [21]. In this study, we hypothesised that the capacity of hookworms and whipworms to establish infection successfully might be related to the types of metabolites produced by their infective stages in the lung and gut, respectively. These findings would shed light on whether the metabolomes of infective-stage hookworms and whipworms are conserved or display stage-, species- or niche-specific molecules. Moreover, some of the metabolites discovered herein might be useful as potential diagnostic biomarkers.

2. Results

2. Results

2.1. MSI Level-1 Identification of Polar Metabolites Present in the Infective Stages of N. brasiliensis and T. muris

2.1. MSI Level-1 Identification of Polar Metabolites Present in the Infective Stages of N. brasiliensis and T. muris

Using an untargeted LC-MS protocol, we analysed the metabolome composition of the infective stages of *N. brasiliensis* and *T. muris* as outlined in the Methods (Figure 1). From the infective L3 stage of *N. brasiliensis*, we prepared two biological samples—somatic tissue extract and ESP—and each biological sample had five replicates. The replicates of the L3 somatic tissue extract were named NB_SE_1 through NB_SE_5; ESP replicates were named NB_ESP_1 through NB_ESP_5. From the infective embryonated eggs of *T. muris*, we prepared five replicates of the somatic tissue extract, which were named TM_SE_1 through TM_SE_5. For the quality control, we prepared a pooled quality control from the samples (QC_P_1–QC_P_3) and media control (QC_Media_1–QC_Media_3) from the same media used for the experimental cultures. Using Metabolomics Standards Initiative level-2 (MSI-II) identification based on accurate mass and predicted retention time, using the open-source software IDEOM (an Excel interface for analysis of LC-MS-based metabolomic data), we identified a total of 164 putative polar metabolites altogether (i.e., after subtracting media peak area values from each metabolite) (Supplementary Table S1 from three different samples (NB_SE, NB_ESP and TM_SE). Most of the polar metabolites were the products of amino acid metabolism, followed by carbohydrate metabolism and nucleotide metabolism (Figure 2A–C).

Using an untargeted LC-MS protocol, we analysed the metabolome composition of the infective stages of *N. brasiliensis* and *T. muris* as outlined in the Methods (Figure 1). From the infective L3 stage of *N. brasiliensis*, we prepared two biological samples—somatic tissue extract and ESP—and each biological sample had five replicates. The replicates of the L3 somatic tissue extract were named NB_SE_1 through NB_SE_5; ESP replicates were named NB_ESP_1 through NB_ESP_5. From the infective embryonated eggs of *T. muris*, we prepared five replicates of the somatic tissue extract, which were named TM_SE_1 through TM_SE_5. For the quality control, we prepared a pooled quality control from the samples (QC_P_1–QC_P_3) and media control (QC_Media_1–QC_Media_3) from the same media used for the experimental cultures. Using Metabolomics Standards Initiative level-2 (MSI-II) identification based on accurate mass and predicted retention time, using the open-source software IDEOM (an Excel interface for analysis of LC-MS-based metabolomic data), we identified a total of 164 putative polar metabolites altogether (i.e., after subtracting media peak area values from each metabolite) (Supplementary Table S1 from three different samples (NB_SE, NB_ESP and TM_SE). Most of the polar metabolites were the products of amino acid metabolism, followed by carbohydrate metabolism and nucleotide metabolism (Figure 2A–C).

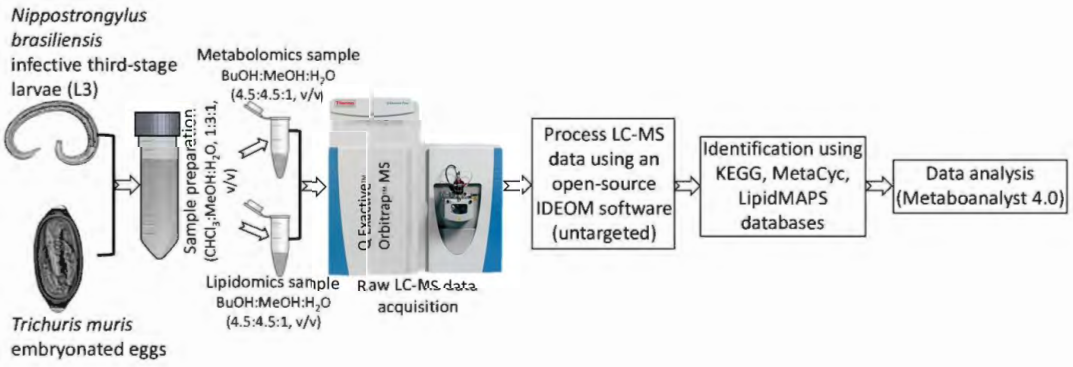

Figure 1. Schematic flowchart of the metabolomic and lipidomic profiling strategy applied for the infective stages of the *N. brasiliensis* (L3) and *T. muris* (embryonated eggs).

Figure 1. Schematic flowchart of the metabolomic and lipidomic profiling strategy applied for the infective stages of the *N. brasiliensis* (L3) and *T. muris* (embryonated eggs).

Of these 164 putative polar metabolites, authentic chemical standards were available for 55 metabolites, allowing confident identification of 55 polar metabolites by accurate mass and retention time (MSI-I identification) (Table 1). Of the 55 metabolites, 21 were common to all three samples (NB_SE, NB_ESP, and TM_SE), comprising mostly products of amino acid metabolism, followed by carbohydrate and nucleotide metabolism. Based on the intensity of peak areas, adenosine, betaine, adenine, lactose, and choline were the top five compounds present in NB_SE. In NB_ESP, betaine, (S)-malate, L-glutamine, isocitrate, and 5-oxoproline were present as the major compounds. TM_SE contained L-leucine, lactose, adenosine, L-proline, and urocanate as the major metabolites (Table 1).

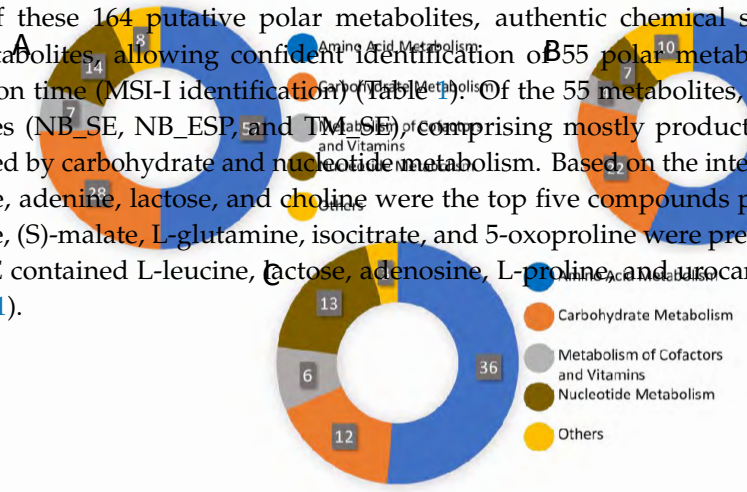

Figure 2. Distribution of total putative metabolites by different metabolite classes (**A**) in the somatic extract of infective third-stage larvae (L3) of *N. brasiliensis* (NB_SE); (**B**) in the excretory/secretory

Table 1. Polar metabolites (MSI-I identified) of infective stages of *N. brasiliensis* (L3) and *T. muris* (embryonated eggs).

Polar Metabolites	Formula [a]	Mass (*m*/*z*)	Rt (min) [c]	KEGG ID [d]	Log_2(FC) [e]	Chemical Taxonomy [b]	Reported Pharmacological Activities	Average Peak Area (mz/rt)		
								NB_SE	NB_ESP	TM_SE
Adenine	$C_5H_5N_5$	135.054	8.32	C00147	5.23	6-aminopurines	Anti-inflammatory [32]	103,160,746	309,024	101,274
Adenosine	$C_{10}H_{13}N_5O_4$	267.096	8.23	C00212	5.21	Purine nucleosides	Anti-inflammatory [33]	327,057,005	0	347,270
Inosine	$C_{10}H_{12}N_4O_5$	268.080	10.32	C00294	4.77	Purine nucleosides	Anti-inflammatory [34,35]	14,631,676	0	18,472
L-Carnitine	$C_7H_{15}NO_3$	161.105	12.32	C00487	4.56	Carnitines	Anti-inflammatory [36] and anti-oxidant [37]	81,471,762	1,911,162	125,132
Choline	$C_5H_{13}NO$	103.099	20.72	C00114	4.53	Cholines	Anti-inflammatory [38]	82,418,790	0	129,808
N(pi)-Methyl-L-histidine	$C_7H_{11}N_3O_2$	169.085	11.58	C01152	3.86	Histidine and derivatives	N/A	5,268,444	2,170,489	13,260
Xanthine	$C_5H_4N_4O_2$	152.033	11.08	C00385	3.62	Xanthines	Proinflammatory [39]	37,256,722	3,609,773	103,264
L-Aspartate	$C_4H_7NO_4$	133.037	14.57	C00402	3.52	Aspartic acid and derivatives	Anti-inflammatory and neuroprotective [40,41]	3,886,437	402,353	9321
Succinate	C4H6O4	118.026	15.15	C00042	3.14	Dicarboxylic acids and derivatives	Activate inflammatory pathways [42,43]	29,148,318	5,130,431	99,396
5-Aminolevulinate	$C_5H_9NO_3$	131.058	13.74	C00430	3.11	Delta amino acids and derivatives	Anti-inflammatory [44]	8,231,888	0	33,627
Adenosine 5′-monophosphate	$C_{10}H_{14}N_5O_7P$	347.063	13.03	C00020	3.05	Purine ribonucleoside monophosphates	Anti-inflammatory [45,46]	9,485,566	0	43,938
Hypoxanthine	$C_5H_4N_4O$	136.038	9.56	C00262	2.84	Hypoxanthines	Anti-inflammatory and wound healing [47]	48,567,229	425,871	230,726
Lactose	$C_{12}H_{22}O_{11}$	342.116	15.25	C00243	2.61	O-glycosyl compounds	N/A	94,498,840	420,550	552,215
L-Glutamate	$C_5H_9NO_4$	147.053	14.24	C00025	2.30	Glutamic acid and derivatives	Antioxidant [48]	16,940,920	4,993,538	104,717
L-Methionine	$C_5H_{11}NO_2S$	149.051	10.81	C00073	2.06	Methionine and derivatives	Anti-inflammatory [49] and antioxidant [50]	2,078,174	890,947	15,017
L-Histidine	$C_6H_9N_3O_2$	155.069	14.25	C00135	1.82	Histidine and derivatives	Anti-inflammatory [51]	14,964,799	1,089,738	135,916
4-Hydroxybenzoate	$C_7H_6O_3$	138.031	10.37	C00156	1.73	Hydroxybenzoic acid derivatives	Neuroprotective [52]	1,566,927	1,019,203	13,620

Table 1. *Cont.*

Polar Metabolites	Formula [a]	Mass (*m*/*z*)	Rt (min) [c]	KEGG ID [d]	Log_2(FC) [e]	Chemical Taxonomy [b]	Reported Pharmacological Activities	Average Peak Area (mz/rt)		
								NB_SE	NB_ESP	TM_SE
L-Tyrosine	$C_9H_{11}NO_3$	181.074	12.44	C00082	1.09	Tyrosine and derivatives	N/A	3,708,634	6,686,668	58,822
Deoxyadenosine	$C_{10}H_{13}N_5O_3$	251.101	7.48	C00559	−1.03	Purine 2′-deoxyribonucleosides	Cell growth inhibitor and cytotoxic [53]	628,485	0	39,096
(S)-Malate	$C_4H_6O_5$	134.021	16.18	C00149	−1.28	Beta hydroxy acids and derivatives	N/A	51,344,999	43,880,026	0
D-Glucose 6-phosphate	$C_6H_{13}O_9P$	260.029	15.83	C00092	−1.66	Hexose phosphates	N/A	402,720	0	42,982
2-Oxoglutarate	$C_5H_6O_5$	146.021	15.77	C00026	−1.80	Gamma-keto acids and derivatives	Anti-inflammatory [54] and antioxidant [55]	249,067	2,843,652	0
L-Pipecolate	$C_6H_{11}NO_2$	129.079	11.42	C00408	−1.94	L-alpha-amino acids	N/A	139,920	0	16,319
Mannitol	$C_6H_{14}O_6$	182.079	13.30	C00392	−2.08	Sugar alcohol	Anti-edema [56]	299,808	0	37,781
L-Alanine	$C_3H_7NO_2$	89.047	14.12	C00041	−2.27	L-alpha-amino acids	Anti-inflammatory [57–59]	3,102,359	3,529,005	0
Betaine	$C_5H_{11}NO_2$	117.079	10.39	C00719	−2.39	Alpha amino acids	Neuroprotective [60]; improves intestinal barrier function [61]; hepatoprotective [62]; anti-inflammatory [38]	261,777,360	56,072,188	0
L-Lysine	$C_6H_{14}N_2O_2$	146.105	22.50	C00047	−2.45	L-alpha-amino acids	Anti-inflammatory [63,64]	2,260,735	1,941,102	0
L-Arginine	$C_6H_{14}N_4O_2$	174.111	24.05	C00062	−2.47	L-alpha-amino acids	Anti-inflammatory [65–67]	30,934,546	3,589,173	0
L-Glutamine	$C_5H_{10}N_2O_3$	146.069	14.44	C00064	−2.48	L-alpha-amino acids	Anti-inflammatory [57–59]	45,487,251	39,780,748	0
L-2-Aminoadipate	$C_6H_{11}NO_4$	161.068	14.47	C00956	−2.49	L-alpha-amino acids	N/A	137,122	0	22,389
L-Phenylalanine	$C_9H_{11}NO_2$	165.079	9.35	C00079	−2.50	L-alpha-amino acids	Anti-diabetic [68]	1,534,294	18,355,000	0
3′,5′-Cyclic AMP	$C_{10}H_{12}N_5O_6P$	329.052	8.72	C00575	−2.54	3′,5′-cyclic purine nucleotides	Anti-inflammatory [69]	281,873	0	57,179
N-Acetylputrescine	$C_6H_{14}N_2O$	130.110	21.02	C02714	−2.58	Carboximidic acids	Lung cancer biomarker [70]	125,036	0	22,355
Thymine	$C_5H_6N_2O_2$	126.043	6.96	C00178	−3.62	Hydroxypyrimidines	N/A	169,388	0	64,297
L-Leucine	$C_6H_{13}NO_2$	131.094	9.97	C00123	−4.14	Leucine and derivatives	Analgesic and anti-inflammatory [71,72]	1,593,314	10,121,672	735,972
Urocanate	$C_6H_6N_2O_2$	138.043	10.49	C00785	−4.16	Imidazolyl carboxylic acids and derivatives	Chemoattractant [73]	452,897	169,049	232,883

Table 1. *Cont.*

Polar Metabolites	Formula [a]	Mass (*m*/*z*)	Rt (min) [c]	KEGG ID [d]	Log_2(FC) [e]	Chemical Taxonomy [b]	Reported Pharmacological Activities	Average Peak Area (mz/rt)		
								NB_SE	NB_ESP	TM_SE
Azelaic acid	$C_9H_{16}O_4$	188.105	10.69	C08261	−4.89	Medium-chain fatty acids	Anti-inflammatory [74]	131,028	874,645	116,635
Maleic acid	$C_4H_4O_4$	116.011	12.18	C01384	−5.67	Dicarboxylic acids and derivatives	Inflammatory/Cytotoxic [75]	98,623	0	154,549
D-Glycerate	$C_3H_6O_4$	106.026	11.85	C00258	ns	Sugar acids and derivatives	N/A	343,824	0	8833
Homogentisate	$C_8H_8O_4$	168.042	9.42	C00544	ns	2(hydroxyphenyl)acetic acids	Pro-inflammatory [76,77]	0	640,416	0
Isocitrate	$C_6H_8O_7$	192.027	19.04	C00311	ns	Tricarboxylic acids and derivatives	N/A	0	37,798,044	0
L-Citrulline	$C_6H_{13}N_3O_3$	175.095	14.84	C00327	ns	L-alpha-amino acids	Anti-inflammatory and antioxidant [78–80]	672,469	0	21,477
L-Proline	$C_5H_9NO_2$	115.063	11.96	C00148	ns	Proline and derivatives	Anti-inflammatory [81]	9,760,345	1,106,588	269,125
L-Serine	$C_3H_7NO_3$	105.042	15.56	C00065	ns	Serine and derivatives	Modulates adaptive immunity by controlling T cell proliferative capacity [82]; colon protection and mucosal healing [81]	337,344	45,878	6178
L-Threonine	$C_4H_9NO_3$	119.058	14.14	C00188	ns	L-alpha-amino acids	Anti-inflammatory [83,84]	425,688	0	14,375
L-Tryptophan	$C_{11}H_{12}N_2O_2$	204.090	11.03	C00078	ns	Indolyl carboxylic acids and derivatives	Anti-inflammatory [85–87]	2,002,647	1,435,161	127,849
L-Valine	$C_5H_{11}NO_2$	117.079	11.76	C00183	ns	Valine and derivatives	Anti-inflammatory [85]	474,387	9,518,904	25,791
LL-2,6-Diaminoheptanedioate	$C_7H_{14}N_2O_4$	190.095	17.63	C00666	ns	Amino acid	N/A	0	115,608	0
N6,N6,N6-Trimethyl-L-lysine	$C_9H_{20}N_2O_2$	188.152	21.12	C03793	ns	L-alpha-amino acids	Cardiovascular disease biomarker [88]	462,527	208,659	12,965
Orotate	$C_5H_4N_2O_4$	156.017	10.27	C00295	ns	Pyrimidinecarboxylic acids	N/A	0	437,266	0
Pterin	$C_6H_5N_5O$	163.049	10.30	C00715	ns	Pterins and derivatives	Biomarker of exercise-induced stress [89]	0	460,935	0

Table 1. *Cont.*

Polar Metabolites	Formula [a]	Mass (*m*/*z*)	Rt (min) [c]	KEGG ID [d]	Log_2(FC) [e]	Chemical Taxonomy [b]	Reported Pharmacological Activities	Average Peak Area (mz/rt)		
								NB_SE	NB_ESP	TM_SE
Pyridoxal	$C_8H_9NO_3$	167.058	7.46	C00250	ns	Pyridoxals and derivatives	N/A	323,537	0	10,226
5-Oxoproline	$C_5H_7NO_3$	129.042	9.82	C01879	ns	Alpha amino acids and derivatives	Promotes oxidative stress in neuropathology [90]	0	32,495,730	0
2,5-Dihydroxybenzoate	$C_7H_6O_4$	154.026	8.30	C00628	ns	Hydroxybenzoic acid derivatives	Anti-cancer activity [91]	0	1,377,617	0
4-Trimethylammoniobutanoate	$C_7H_{15}NO_2$	145.110	12.25	C01181	ns	Straight chain fatty acids	N/A	217,954	0	2264

[a] Formula; [b] Chemical taxonomy = Formula and chemical taxonomy for compounds were taken from human metabolome database (HMDB, http://www.hmdb.ca); [c] Rt = retention time in minutes; [d] KEGG ID (http://www.genome.jp/kegg/) contains information on biosynthetic and metabolic pathways of identified compounds; [e] log 2(FC) is a fold change between NB_SE and TM_SE; Abbreviations: ns = not significant; ID = identity; NB_SE = the somatic extract of infective third-stage larvae (L3) of *N. brasiliensis*; NB_ESP = the excretory/secretory products (ESP) of *N. brasiliensis* L3; TM_SE = the somatic extract of *T. muris* embryonated eggs. Note: peak areas values of media were subtracted from the samples.

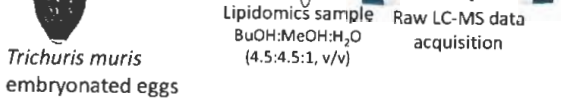

Figure 1. Schematic flowchart of the metabolomic and lipidomic profiling strategy applied for the infective stages of the *N. brasiliensis* (L3) and *T. muris* (embryonated eggs).

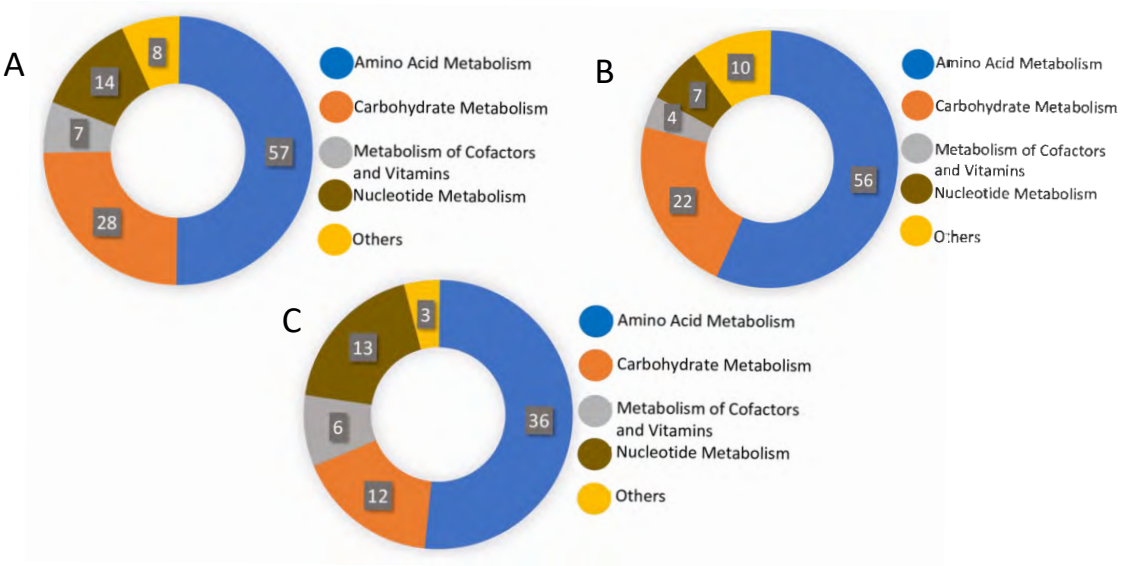

Figure 2. Distribution of total putative metabolites by different metabolite classes (**A**) in the somatic extract of infective third-stage larvae (L3) of *N. brasiliensis* (NB_SE); (**B**) in the excretory/secretory products of *N. brasiliensis* L3 (NB_ESP); and (**C**) in the somatic extract of *T. muris* embryonated eggs (TM_SE).

2.2. Metabolic Pathways of Putatively Identified Polar Metabolites

Based on the 164 putative polar metabolites identified from the three biological samples (114 metabolites from NB_SE, 99 from NB_ESP, 70 from TM_SE), we deduced metabolic pathways (MAPs) by mapping all the compounds against known metabolite pathways for helminths in the Kyoto Encyclopedia of Genes and Genomes (KEGG), Human Metabolome Database (HMDB), and MetaCyc Metabolic Pathway database. In all three sample groups, the highest number of identified metabolites/compounds were products of amino acid metabolism, followed by carbohydrate metabolism in NB_SE and NB_ESP, and nucleotide metabolism in TM_SE, as shown in Figure 2A–C. For example, of 114 metabolites identified from the NB_SE, 57 metabolites were produced through amino acid metabolism, 28 by carbohydrate metabolism, and 14 by nucleotide metabolism. A similar pattern can be seen in its ESP. Of 70 polar metabolites identified from TM_SE, 36 of them were the products of amino acid metabolism, 13 were from nucleotide metabolism, and 12 were from carbohydrate metabolism.

2.3. Chemometric Analysis of the Polar Metabolites of N. brasiliensis L3 and T. muris Embryonated Eggs

We performed statistical analysis on the 55 polar metabolites identified in Table 1 (MSI-I identification) using MetaboAnalysis 4 (http://www.metaboanalyst.ca) to determine metabolite differences. First, the differences in the abundance of polar metabolites between NB_SE and TM_SE were evaluated by univariate analysis (volcano plot analysis). NB_ESP was excluded from the univariate analysis since there was no ESP from the infective stage of *T. muris*. Volcano plot analysis identified differential metabolites using the *t*-test and fold-change (FC) methods, and we plotted $\log_2$ (fold-change > 2) on the *X*-axis against $-log_{10}$ (*p*-value) from the *t*-test on the *Y*-axis. Benjamini–Hochberg correction or false discovery rate was applied to compute the number of false positives out of significantly varied metabolic features. Table 1 shows the fold change and the *p*-values of these significantly different metabolites. When we compared NB_SE metabolites against TM_SE, 38 of 49 (approximately 78%) metabolites showed significant differences ($p < 0.05$), where both the samples (i.e., NB_SE and TM_SE) had 19 metabolites each with an absolute log2 fold change > 2 and an absolute *p*-value < 0.05 (represented as pink dots in Figure 3).

We next performed multivariate analysis by a principal component analysis (PCA) and hierarchical clustering analyses (with heat-map analyses) to determine the overall metabolic similarities and

Kyoto Encyclopedia of Genes and Genomes (KEGG), Human Metabolome Database (HMDB), and MetaCyc Metabolic Pathway database. In all three sample groups, the highest number of identified metabolites/compounds were products of amino acid metabolism, followed by carbohydrate metabolism in NB_SE and NB_ESP, and nucleotide metabolism in TM_SE, as shown in Figure 2A–C. For example, of 114 metabolites identified from the NB_SE, 57 metabolites were produced through amino acid metabolism, 28 by carbohydrate metabolism, and 14 by nucleotide metabolism. A similar pattern can be seen in its ESP. Of 70 polar metabolites identified from TM_SE, 36 of them (Figure 4) were products of amino acid metabolism, 13 were from nucleotide metabolism, and 12 were from carbohydrate metabolism.

2.3. Chemometric Analysis of the Polar Metabolites of *N. brasiliensis* L3 and *T. muris* Embryonated Eggs

We performed statistical analysis on the 55 polar metabolites identified in Table 1 (MSI-1 identification) using MetaboAnalysis 4 (http://www.metaboanalyst.ca) to determine metabolite differences. First, the differences in the abundance of polar metabolites between NB_SE and TM_SE were evaluated by univariate analysis (volcano plot analysis). NB_ESP was excluded from the univariate analysis since there was no ESP from the infective stage of *T. muris*. Volcano plot analysis identified differential metabolites using the *t*-test and fold-change (FC) methods, and we plotted $\log_2$ (fold-change > 2) on the *X*-axis against $-\log_{10}$ (*p*-value) from the *t*-test on the *Y*-axis. Benjamini–Hochberg correction of false discovery rate was applied to compute the number of false positives out of significantly varied metabolic features. Table 1 shows the fold change and the *p*-values of these significantly different metabolites. When we compared NB_SE metabolites against TM_SE, 38 of 49 (approximately 78%) metabolites showed significant differences ($p < 0.05$), where both the samples (i.e., NB_SE and TM_SE) had 19 metabolites each with an absolute log2 fold change > 2 and an absolute *p*-value < 0.05 (represented as pink dots in Figure 3).

Additionally, we used hierarchical clustering heat-map analysis (distance measured by Euclidean and clustering algorithm using ward.D) to evaluate the difference in the concentration of each metabolite between sample groups. Clustered heat-maps allow easy visualisation of changing patterns in metabolite concentrations across sample groups and experimental conditions. The metabolite pattern of each biological replicate from three sample groups clustered, and individual clusters were distinct, indicating the uniqueness of the metabolome profiles of the two helminths. Unlike score plots, heat-maps display the actual data values using carefully chosen colour gradients, as shown in Figure 5, where blue bars indicate a low concentration and red bar denotes a high concentration. Based on the colour intensity pattern in the heat-map, adenine (purine nucleobase), adenosine (purine nucleoside), choline (amino acid), and hypoxanthine were notable features in the NB_SE. Amino acids such as L-tyrosine, L-valine, 2-oxoglutarate, L-phenylalanine, and 4-hydroxybenzoate were prominent in NB_ESP. In TM_SE, L-2-aminoadepate, L-pipecolate, and N-acetylputrescine (amino acids), thymine (nucleic acid), and maleic acid (organic acid) were prominent.

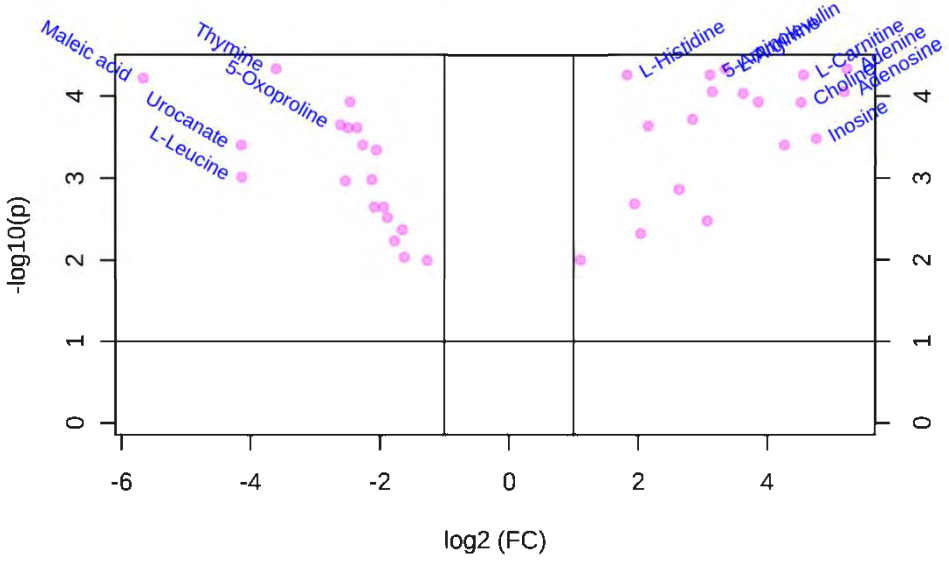

Figure 3. Volcano plot of untargeted metabolomics analysis of differential features (i.e., 49 MSI-1 (Metabolomics Standard Initiative level-1) identified polar metabolites from somatic extracts) between the extract of infective third-stage larvae (L3) of *N. brasiliensis* (NB_SE) and the extract of *T. muris* embryonated eggs (TM_SE). The plot displays log2 fold changes versus Benjamini–Hochberg adjusted *p*-values (−log10 transformed). Features that exhibited log2 fold change > 2 and an absolute *p*-value < 0.05 are coloured in pink. Most significant metabolites are labelled with the corresponding name.

similarities and differences between three sample groups (i.e., NB_SE, NB_ESP, and TM_SE). As expected, the PCA plot (Figure 4) showed a clear separation among the three biological groups, indicating that the infective stages of the two STHs (*N. brasiliensis* and *T. muris*) produce distinct metabolite profiles. The plot shows that the variation of metabolites between the different helminth species and the difference shown on PC1 was greater than the difference between somatic extract and excretory/secretory product.

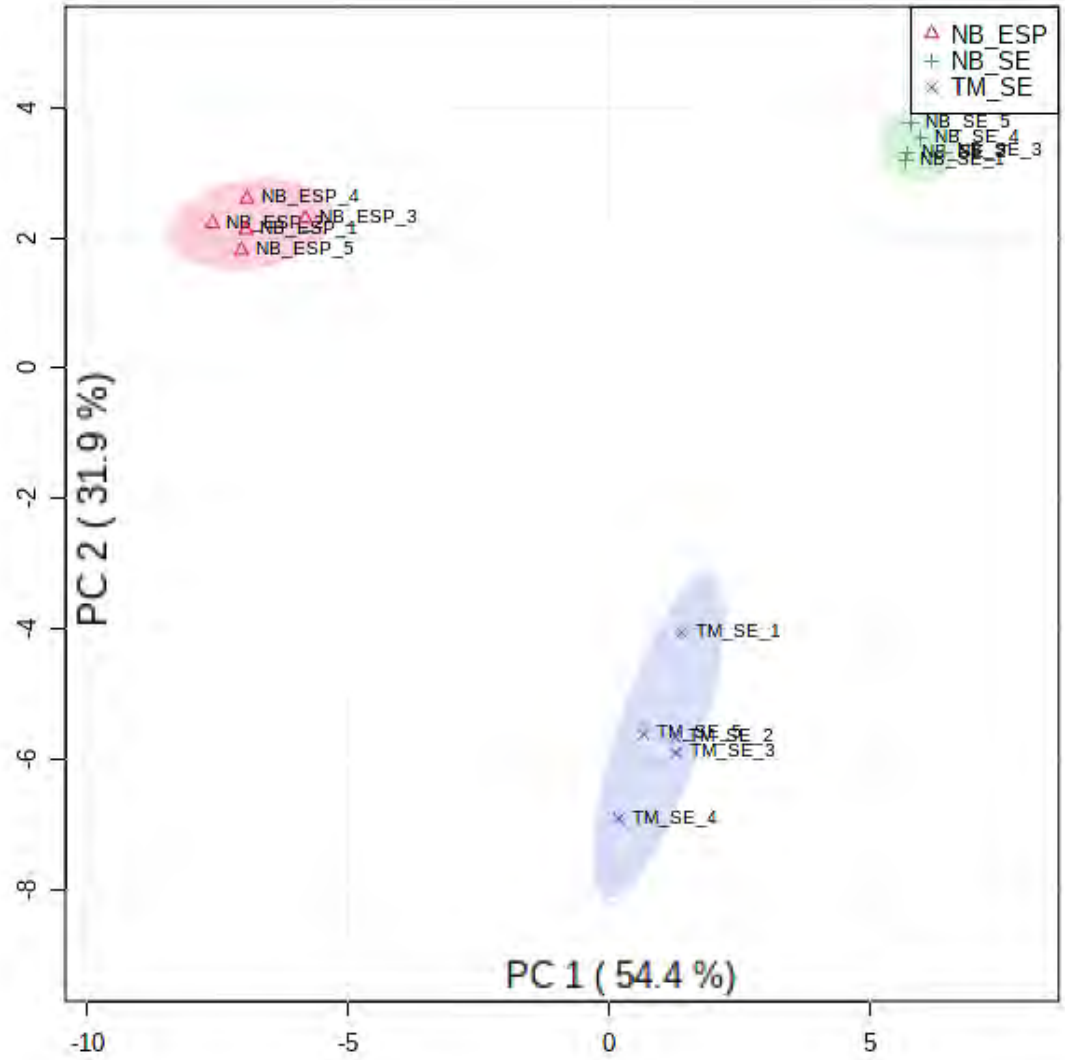

Figure 4. Principal component analysis scores plot for the sample groups, i.e., the somatic extract of infective third stage larvae (L3) of *N. brasiliensis* (NB_SE) (green), excretory/secretory products (ESP) of *N. brasiliensis* L3 (NB_ESP) (red), and the somatic extract of *T. muris* embryonated eggs (TM_SE) (blue) with five replicates each. Parentheses on each axis explain the amount of variance. Media (QC_Media) and pooled quality control (QC_P) values were excluded from the analysis, as they were subtracted from the samples.

Additionally, we used hierarchical clustering heat-map analysis (distance measured by Euclidean, and clustering algorithm using ward.D) to evaluate the difference in the concentration of each metabolite between sample groups. Clustered heat-maps allow easy visualisation of changing patterns in metabolite concentrations across sample groups and experimental conditions. The

concentration. Based on the colour intensity pattern in the heat-map, adenine (purine nucleobase), adenosine (purine nucleoside), choline (amino acid), and hypoxanthine were notable features in the NB_SE. Amino acids such as L-tyrosine, L-valine, 2-oxoglutarate, L-phenylalanine, and 4-hydroxybenzoate were prominent in NB_ESP. In TM_SE, L-2-aminoadepate, L-pipecolate, and N-acetylputrescine (amino acids), thymine (nucleic acid), and maleic acid (organic acid) were prominent.

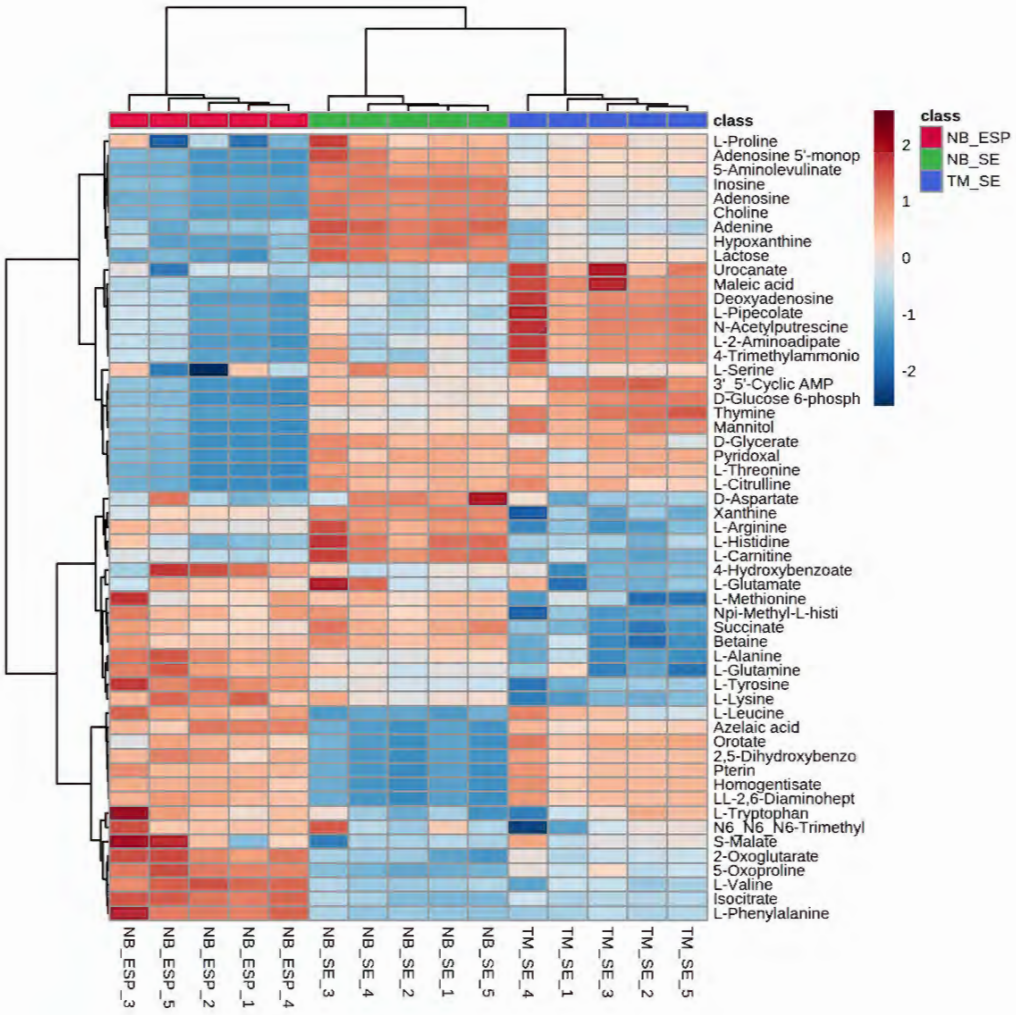

Figure 5. Hierarchical clustering analysis (HCA) of the three samples (the somatic extract of infective third-stage larvae (L3) of *N. brasiliensis* (NB_SE), the excretory/secretory products (ESP) of *N. brasiliensis* L3 (NB_ESP), and the somatic extract of *T. muris* embryonated eggs (TM_SE)) showing discrimination between the sample types and differential abundances of 55 polar metabolites. Each column represents sample groups with their replicates, and each row represents the expression profile of a metabolite across sample groups. The scale bar represents the normalised intensity of metabolites; where blue indicates a decrease/low and red an increase/high. Media (QC_Media) and pooled quality control (QC_P) values were excluded from the analysis, as they were subtracted from the samples.

2.4. Lipidomics Analysis of the *N. brasiliensis* and *T. muris* Infective Stages

After acquiring LC-MS data (mass and retention time) using open source software IDEOM, lipids were putatively identified by accurate mass within 3 ppm. We putatively identified (MSI level-2 identification) a total of 350 lipids (Supplementary Table S2) in all three samples (332 in NB_SE, 256 in NB_ESP, and 283 in TM_SE), out of which 203 lipids were common in all three sample groups. Of the vast array of lipids identified, glycerophospholipids such as phosphatidylcholine (PC) and phosphatidylethanolamine (PE) were predominant in NB_SE. In NB_ESP and TM_SE, glycerolipid triglycerides (TG) were present in higher intensities. Based on their intensity of peak areas, glycerophospholipid species phosphatidylcholine (PC) such as PC(38:6), PC(40:5), PC(40:7), PC(40:8), and PC(40:9) were the top five lipids in NB_SE. In NB_ESP and TM_SE, glycerolipid species such as triglyceride (TG) were dominant. TG(48:1), TG(45:0), TG(50:2), TG(47:1), and TG(52:2) were the top five lipids in NB_ESP and TG(30:0), TG(38:0), TG(38:1), TG(40:0), and TG(42:1) in TM_SE.

triglycerides (TG) were present in higher intensities. Based on their intensity of peak areas, glycerophospholipid species phosphatidylcholine (PC) such as PC(38:6), PC(40:5), PC(40:7), PC(40:8), and PC(40:9) were the top five lipids in NB_SE. In NB_ESP and TM_SE, glycerolipid species such as triglyceride (TG) were dominant. TG(48:1), TG(45:0), TG(50:2), TG(47:1), and TG(52:2) were the top five lipids in NB_ESP and TG(30:0), TG(38:0), TG(38:1), TG(40:0), and TG(42:1) in TM_SE.

2.5. Lipidomic Pathways of Identified Lipids

2.5. Lipidomic Pathways of Identified Lipids

We mapped lipidomic pathways for putative lipids against known lipid pathways in lipid databases such as LIPID MAPS Lipidomics Gateway (http://www.lipidmaps.org) and LipidBank (http://www.lipidbank.jp). Most lipids in all three sample groups were the glycerophospholipid metabolism pathway products, followed by glycerolipid and fatty acyl metabolism (Figure 6). Elements of glycerophospholipid metabolism such as phosphatidic acid (PA), phosphatidylethanolamine (PE), phosphatidylcholine (PC), phosphatidylserine (PS), and phosphatidylinositol (PI) were major lipid constituents in all three sample groups (NB_SE, NB_ESP, and TM_SE), followed by triacyl-glycerides (TG), the product of the glycerolipid pathway (Supplementary Table S2).

We mapped lipidomic pathways for putative lipids against known lipid pathways in lipid databases such as LIPID MAPS Lipidomics Gateway (http://www.lipidmaps.org) and LipidBank (http://www.lipidbank.jp). Most lipids in all three sample groups were the glycerophospholipid metabolism pathway products, followed by glycerolipid and fatty acyl metabolism (Figure 6). Elements of glycerophospholipid metabolism such as phosphatidic acid (PA), phosphatidylethanolamine (PE), phosphatidylcholine (PC), phosphatidylserine (PS), and phosphatidylinositol (PI) were major lipid constituents in all three sample groups (NB_SE, NB_ESP, and TM_SE), followed by triacyl-glycerides (TG), the product of the glycerolipid pathway (Supplementary Table S2).

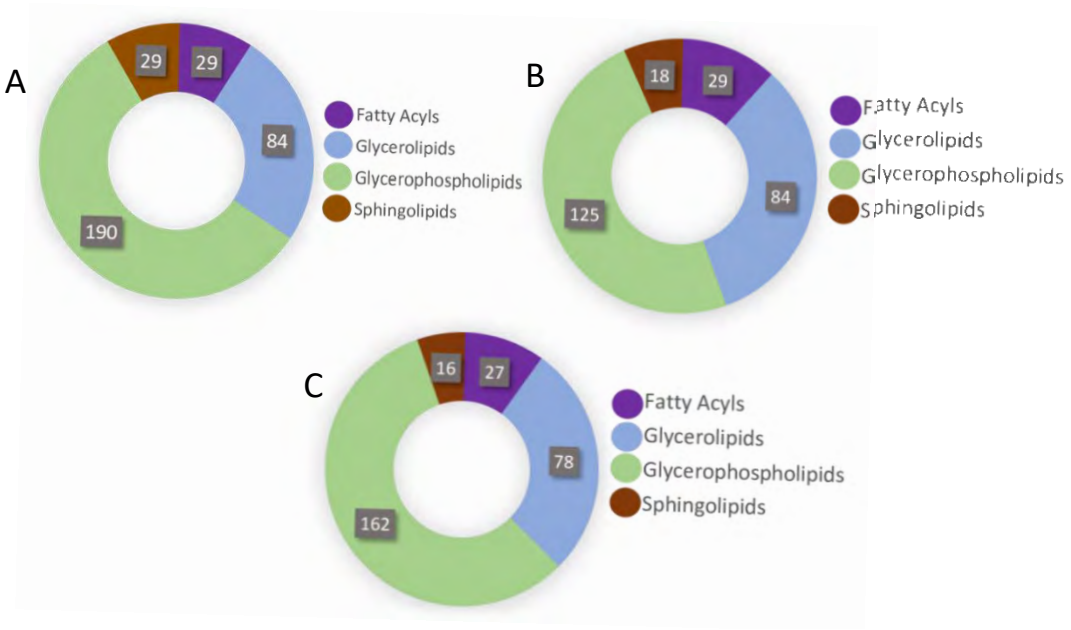

Figure 6. Distribution of putative lipids by lipid classes: (**A**) in the somatic extract of infective third-stage larvae (L3) of *N. brasiliensis* (NB_SE); (**B**) in the excretory/secretory products (ESP) of *N. brasiliensis* L3 stage larvae (L3) of *N. brasiliensis* (NB_SE); (**B**) in the excretory/secretory products (ESP) of *N. brasiliensis* (NB_ESP); (**C**) in the somatic extract of *T. muris* embryonated eggs (TM_SE).

2.6. Chemometric Analysis of Putatively Identified Lipids

2.6. Chemometric Analysis of Putatively Identified Lipids

We performed both univariate and multivariate chemometric analyses using Metaboanalyst 4.0 software, as described above for polar metabolites. For comparison of lipid profiles in the somatic extracts of the infective stages of the two helminths, univariate analysis (volcano plot analysis) between NB_SE and TM_SE yielded 204 significant features out of top 350 lipids (represented by pink dots in Figure 7). All features presented possessed values above a given count threshold (>75% of pairs/variable) and had a fold change of >2 and p-value of <0.05 (Supplementary Table S3). When the NB_SE lipid profile was compared against TM_SE, 10 lipids in NB_SE and five lipids in TM_SE (labelled pink dots in Figure 7) showed the most significant differences in their peak intensities ($p < 0.05$).

We performed both univariate and multivariate chemometric analyses using Metaboanalyst 4.0 software, as described above for polar metabolites. For comparison of lipid profiles in the somatic extracts of the infective stages of the two helminths, univariate analysis (volcano plot analysis) between NB_SE and TM_SE yielded 204 significant features out of top 350 lipids (represented by pink dots in Figure 7). All features presented possessed values above a given count threshold (>75% of pairs/variable) and had a fold change of >2 and p-value of <0.05 (Supplementary Table S3). When the NB_SE lipid profile was compared against TM_SE, 10 lipids in NB_SE and five lipids in TM_SE (labelled pink dots in Figure 7) showed the most significant differences in their peak intensities ($p < 0.05$).

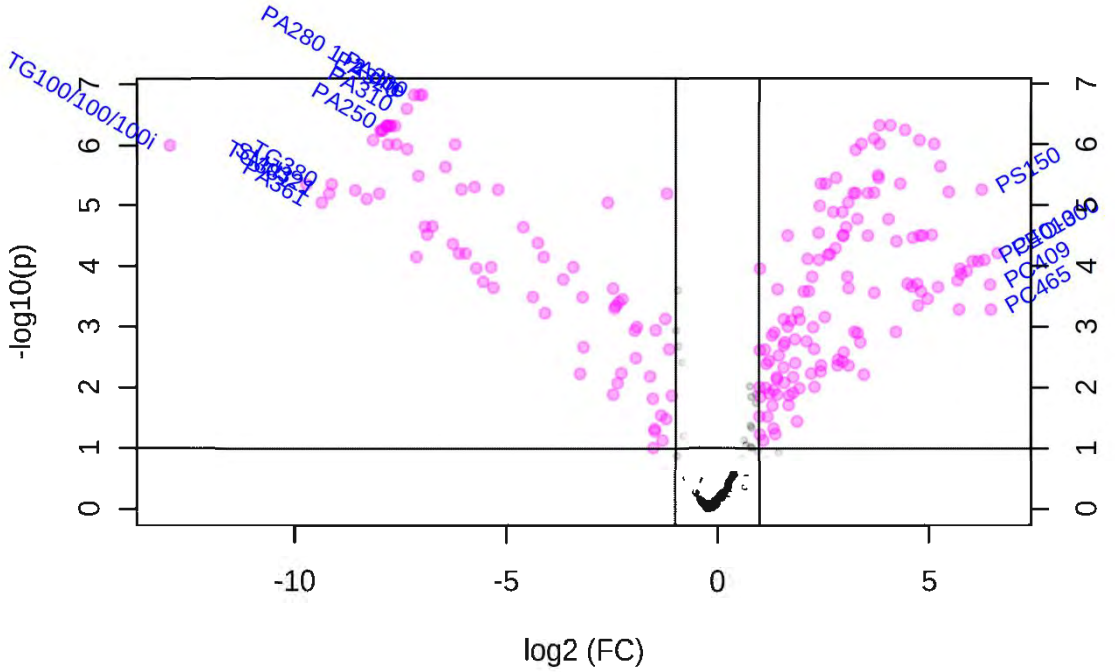

Figure 7. Volcano plot of the untargeted lipidomics analysis of differentially regulated features between the somatic extract of infective third-stage larvae (L3) of *N. brasiliensis* (NB_SE) and the somatic extract of *T. muris* eggs (TM_SE). The volcano plot displays log2 fold changes versus Benjamini–Hochberg adjusted *p*-values (−log10 transformed) (−log10 transformed). Features that exhibited an absolute log_2 fold change > 2 and an adjusted *p*-value < 0.05 are colored in pink. Most significant features which could be structurally annotated are labeled with the corresponding name. Gray dots represent features that were not significantly altered (significant fold change less than 2). The further its position away from the (0,0), the more significant the lipid is.

A principal component analysis of the 350 putative lipids (listed in Supplementary Table S2) showed clear segregation of the clusters among all three sample groups (NB_SE, NB_ESP, and TM_SE) represented in Figure 8. These results indicate a high level of heterogeneity in the lipidomes of the two helminths.

We evaluated the diversity of lipidomic patterns across the three samples by cluster heat map analysis using Metaboanalyst 4.0 statistical analysis package. The variation in the intensities of 350 putative lipids between groups is shown in Figure 9. The somatic extract of *N. brasiliensis* L3 contained a very high intensity of glycerophospholipids such as phosphatidylcholine (PC) and phosphatidylethanolamine (PE) species. Meanwhile, NB_ESP and TM_SE both contained glycerolipids such as triglycerides (TG) species in higher intensities. The Supplementary Table S2 contains the individual intensity of all 350 lipids in each group.

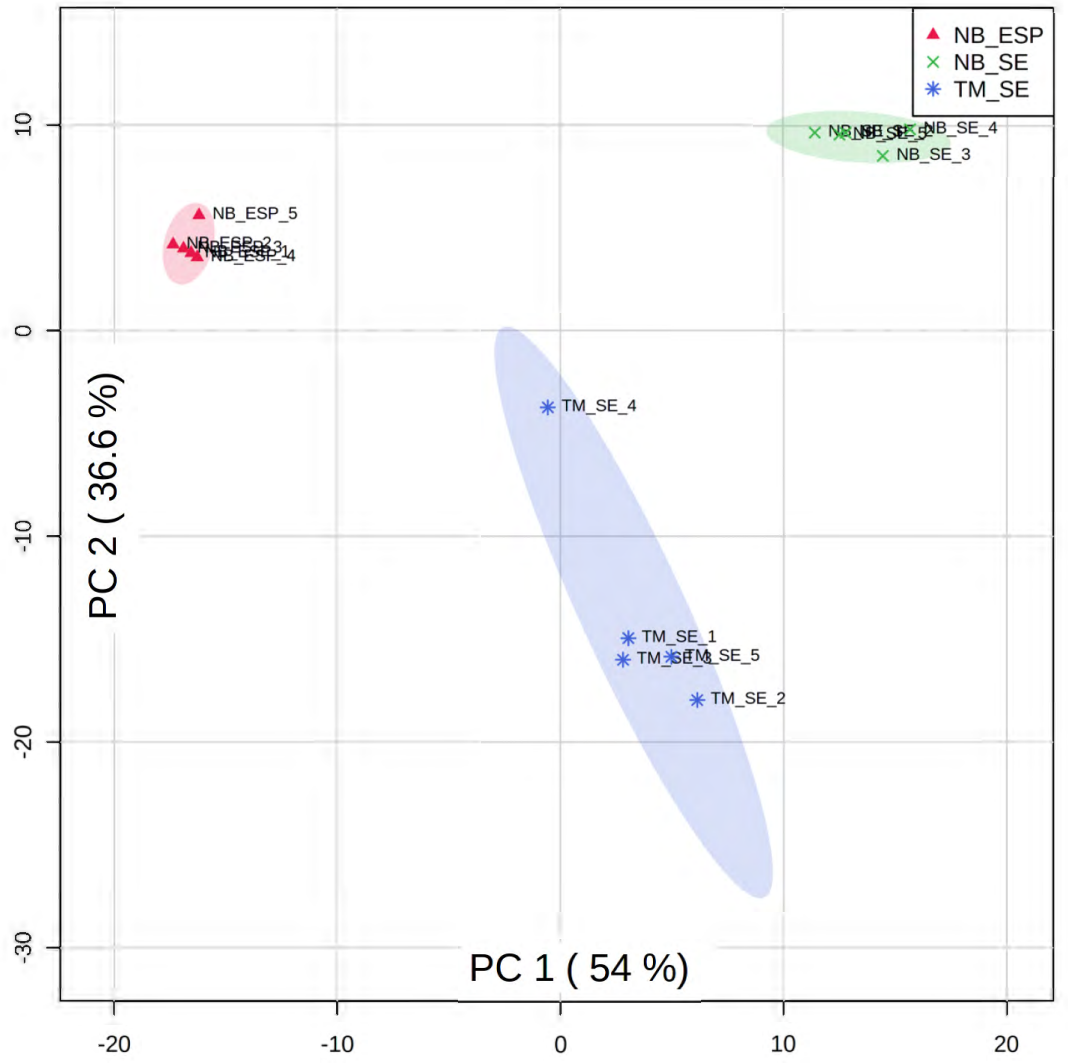

Figure 8. Principal component analysis scores plot comparing LC-MS metabolomic profiles for the lipids among three sample groups: the somatic extract of infective third-stage larvae (L3) of *N. brasiliensis* (NB_SE) (green), the excretory/secretory products of *N. brasiliensis* L3 (NB_ESP) (red), and the somatic extract of *T. muris* embryonated eggs (TM_SE) (blue) with five replicates each. The amount of variance explained is shown in parentheses on each axis. Media (QC_Media) and pooled quality control (QC_P) values were excluded from the analysis, as they were subtracted from the samples.

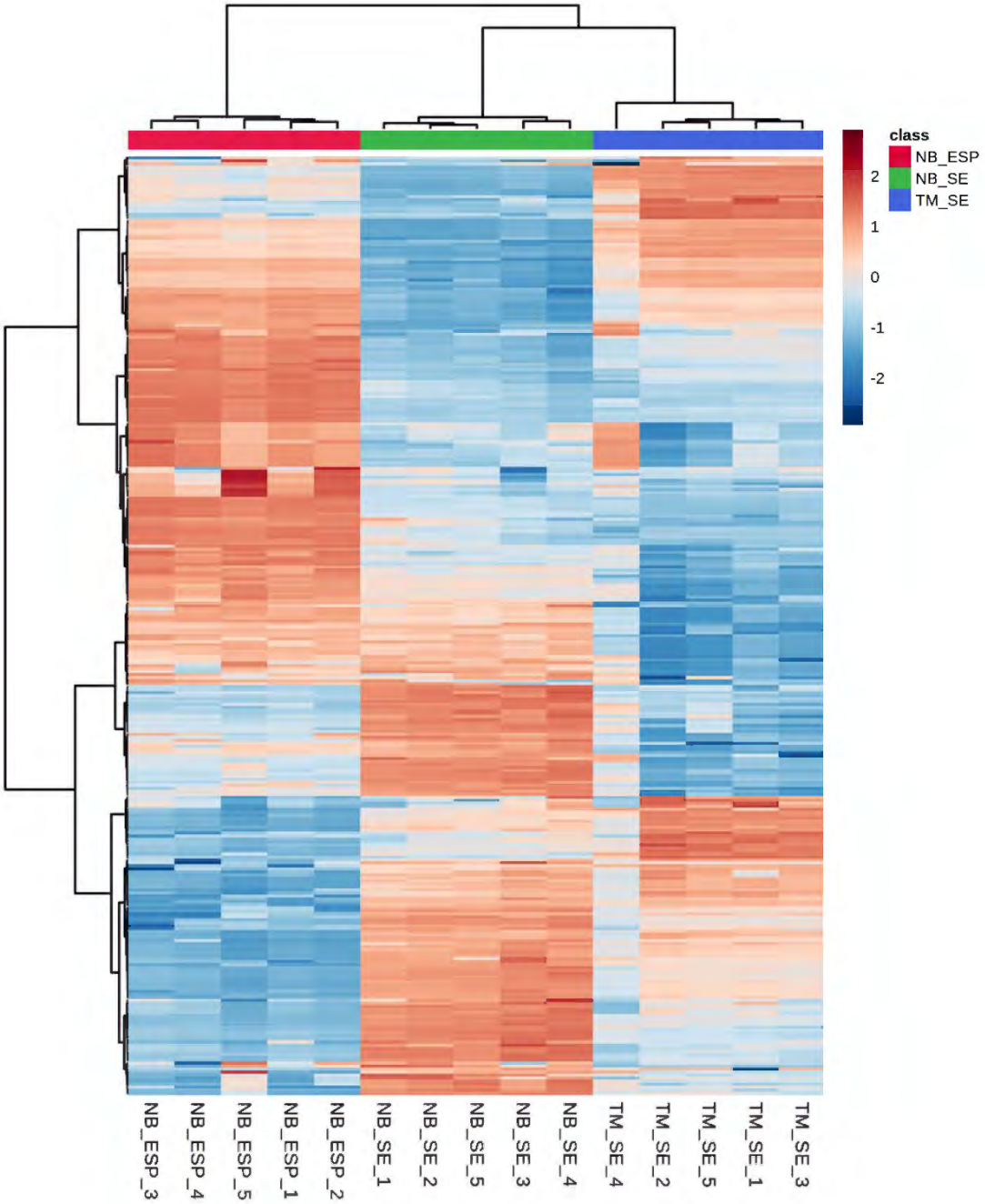

Figure 9. Hierarchical clustering analysis (HCA) of the three samples (the somatic extract of infective third-stage larvae (L3) of *N. brasiliensis* (NB_SE), the excretory/secretory products (ESP) of *N. brasiliensis* L3 (NB_ESP), and the somatic extract of *T. muris* embryonated eggs (TM_SE)), showing discrimination between the sample types and differential abundances of 350 putative lipids. Each row represents putative lipids, and each column represents the biological replicates of an individual sample group. The scale bar represents the normalised intensity of metabolites, where blue colour indicates low/decrease, and red colour indicates high/increase. Media (QC_Media) and pooled quality control (QC_P) values were excluded from the analysis, as they were subtracted from the samples. Note: Heat-map was purposefully generated on all 350 putative lipids to show the overall pattern between the sample groups. For specific lipid details with peak areas, refer to Supplementary Table S2.

2.7. Common and Unique Metabolites in *N. brasiliensis* and *T. muris* Infective Stages

Out of 55 polar metabolites identified in this study, 21 were common to all three sample groups, mostly amino acids. Seven (7) polar metabolites were unique to the ESP of the *N. brasiliensis* infective

2.7. Common and Unique Metabolites in *N. brasiliensis* and *T. muris* Infective Stages

Out of 55 polar metabolites identified in this study, 21 were common to all three sample groups, mostly amino acids. Seven (7) polar metabolites were unique to the ESP of the *N. brasiliensis* infective stage (Table 1 and Figure 10A), and interestingly, two of them, namely isocitrate and 5-oxoproline/pyroglutamic acid, were also detected in their adult ESP [21]. The remaining five, namely homogentisate, orotate, LL-2,6-Diaminoheptanedioate, pterin, and 2,5-dihydroxybenzoate, were absent in the ESP as well as somatic extracts of both helminths. Meanwhile, out of 350 putative lipids identified from all three samples (NB_SE, NB_ESP, and TM_SE), 203 lipids were common to all three sample groups (NB_SE, NB_ESP, and TM_SE). A total of 62 lipids were common between NB_SE and TM_SE, 39 lipids between NB_SE and NB_ESP, and 14 lipids between NB_ESP and TM_SE. Twenty-eight (28) lipids were unique to NB_SE and four lipids to TM_SE (Table 2 and Figure 10B).

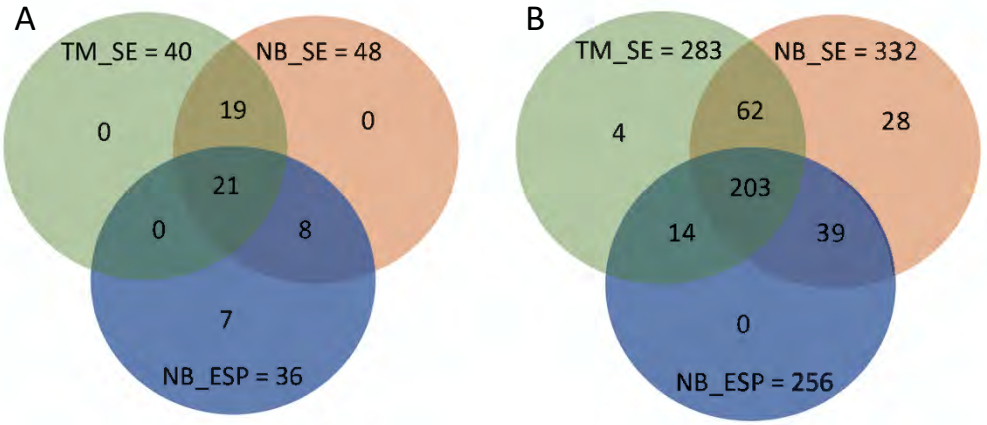

Figure 10. Distribution of common and unique metabolites among the three sample groups: the somatic extract of infective third-stage larvae (L3) of *N. brasiliensis* (NB_SE), the excretory/secretory products (ESP) of *N. brasiliensis* L3 (NB_ESP), and the somatic extract of *T. muris* embryonated eggs (TM_SE). (**A**) MSI-I identified polar metabolites; (**B**) MSI-II identified lipids.

Table 2. Putative lipids unique to infective stages of *N. brasiliensis* (L3) and *T. muris* (embryonated eggs).

Putative Lipids	Formula [a]	Mass (*m/z*)	Rt (min) [c]	Chemical Taxonomy [b]	LipidMAPS ID [d]	Peak Areas (mz/rt)		
						NB_SE	NB_ESP	TM_SE
DG(41:7)	$C_{44}H_{72}O_5$	680.536	16.05	Glycerolipids	LMGL02010545	124,404	0	0
FA hydroxy(12:0) dodecanoic acid	$C_{12}H_{24}O_3$	238.155	2.19	Fatty Acyls	NA	0	0	51,014
LacCer(d38:0)	$C_{50}H_{97}NO_{13}$	919.696	18.98	Sphingolipids	LMSP05010122	139,285	0	0
LacCer(d40:0)	$C_{52}H_{101}NO_{13}$	947.727	20.22	Sphingolipids	LMSP05010124	182,175	0	0
LysoPE(22:2)	$C_{27}H_{52}NO_7P$	533.350	4.84	Glycerophospholipids	LMGP02050024	136,295	0	0
PE-Cer(d40:1)	$C_{42}H_{85}N_2O_7P$	760.610	13.49	Sphingolipids	LMSP03020086	117,114	0	0
PE-Cer(d38:1)	$C_{40}H_{81}N_2O_7P$	732.579	12.26	Sphingolipids	LMSP03020064	112,168	0	0
PA(25:0)	$C_{28}H_{55}O_8P$	550.364	12.05	Glycerophospholipids	LMGP10010001	0	0	374,621
PA(26:0)	$C_{29}H_{57}O_8P$	564.379	12.58	Glycerophospholipids	LMGP10010980	0	0	1,921,006
PC(36:7)	$C_{44}H_{74}NO_8P$	775.514	10.73	Glycerophospholipids	LMGP01012100	105,372	0	0
PC(P-32:2)	$C_{40}H_{76}NO_7P$	713.536	13.07	Glycerophospholipids	NA	657,868	0	0
PC(P-36:2)	$C_{44}H_{84}NO_7P$	769.599	14.95	Glycerophospholipids	LMGP01030137	138,297	0	0
PE(28:2)	$C_{33}H_{62}NO_8P$	631.422	7.68	Glycerophospholipids	LMGP02011238	127,324	0	0
PE(48:2)	$C_{53}H_{102}NO_8P$	911.734	20.75	Glycerophospholipids	LMGP02010893	466,471	0	0
PE(40:5)	$C_{45}H_{80}NO_8P$	815.542	12.76	Glycerophospholipids	LMGP02010893	483,243	0	0
PE(48:1)	$C_{53}H_{104}NO_8P$	913.751	21.37	Glycerophospholipids	NA	1,154,195	0	0
PE(O-20:0)	$C_{25}H_{54}NO_6P$	495.370	7.71	Glycerophospholipids	LMGP02060005	108,008	0	0
PE(P-20:0)	$C_{25}H_{52}NO_6P$	493.354	7.86	Glycerophospholipids	LMGP02070004	375,557	0	0
PE(P-36:4)	$C_{41}H_{74}NO_7P$	723.521	12.51	Glycerophospholipids	LMGP02030093	195,178	0	0
PE(P-36:5)	$C_{41}H_{72}NO_7P$	721.504	11.93	Glycerophospholipids	LMGP02030028	87,036	0	0
PE(P-38:6)	$C_{43}H_{74}NO_7P$	747.519	12.36	Glycerophospholipids	LMGP02030001	308,137	0	0
PG(36:1)	$C_{42}H_{81}O_{10}P$	776.557	11.98	Glycerophospholipids	LMGP04010037	699,995	0	0
PI(37:6)	$C_{46}H_{77}O_{13}P$	868.512	9.51	Glycerophospholipids	LMGP06010790	119,218	0	0
PI(38:7)	$C_{47}H_{77}O_{13}P$	880.512	9.44	Glycerophospholipids	LMGP06010792	168,877	0	0
PI(P-37:2)	$C_{46}H_{85}O_{12}P$	860.576	11.78	Glycerophospholipids	LMGP06030067	94,153	0	0
PS(28:2)	$C_{34}H_{62}NO_{10}P$	675.412	6.97	Glycerophospholipids	LMGP03010919	253,811	0	0
PS(36:4)	$C_{42}H_{74}NO_{10}P$	783.506	10.48	Glycerophospholipids	LMGP03010038	141,937	0	0
PS(36:5)	$C_{42}H_{72}NO_{10}P$	781.491	10.06	Glycerophospholipids	LMGP03010654	115,385	0	0
PS(O-38:0)	$C_{44}H_{88}NO_9P$	805.621	15.40	Glycerophospholipids	LMGP03020051	86,582	0	0
PS(O-34:0)	$C_{40}H_{80}NO_9P$	749.558	12.46	Glycerophospholipids	LMGP03020043	0	0	1883
SM(d41:2)	$C_{46}H_{91}N_2O_6P$	844.667	14.55	Sphingolipids	LMSP03010074	29,023	0	0
SM(d42:2)	$C_{47}H_{93}N_2O_6P$	812.676	15.24	Sphingolipids	LMSP03010007	78,211	0	0

[a] Formula; [b] Chemical taxonomy = Formula and chemical taxonomy for compounds were taken from LipidMAPS database (https://www.LipidMAPS.org); [c] Rt = retention time in minutes; [d] LIPIDMAPS ID (https://www.LipidMAPS.org) contains information on biosynthetic and metabolic pathways of identified lipids; Abbreviations: ID = identity; NB_SE = the somatic extract of infective third-stage larvae (L3) of *N. brasiliensis*; NB_ESP = the excretory/secretory products (ESP) of *N. brasiliensis* L3; TM_SE = the somatic extract of *T. muris* embryonated eggs.

2.8. Reported Pharmacological Activities of Identified Compounds

A comprehensive literature search revealed that 42 out of the 55 polar metabolites were associated with various pharmacological activities. Of the 42 polar metabolites, 31 metabolites possess anti-inflammatory or antioxidant properties (Table 1). For example, polar metabolites such as L-valine (prominent in *N. brasiliensis* ESP), adenine, choline, inosine, adenosine, hypoxanthine (prominent features in *N. brasiliensis* somatic extract), and L-tryptophan (prominent feature in *T. muris* eggs somatic extract) possess anti-inflammatory activity. A few of the detected metabolites were unique to the extracts, such as homogentisate in the *N. brasiliensis* ESP and maleic acid in *T. muris* eggs (embryonated) somatic extract, both (compounds) known for their inflammatory and cytotoxic properties, respectively. Unlike polar metabolites, non-polar metabolites or lipids in helminths are the least studied for biological activities. There is either limited or no record of studies for all putative lipids identified in this study.

3. Discussion

Parasites have co-evolved with humans for millennia and produce ESPs that allow them to navigate through circuitous pathways (for hookworm at least) to reach the gut, where they survive for a prolonged period. STHs are masterful at modulating the host's immune response to avoid elimination from the body and facilitate the establishment of chronic infection [92]. Their ESP contain a plethora of biomolecules, including proteins, peptides, lipids, and other small molecules [21]. However, small molecules remain less-studied, especially those produced by the infective stages. In this study, we show the metabolomes of the infective stages of *N. brasiliensis* and *T. muris* using untargeted LC-MS for the first time. Our results also provide new insights into comparative metabolome profiles of different developmental stages of the helminths. LC-MS is a preferred analytical technique for metabolome profiling [93–95], especially when employing high-resolution accurate mass (HRAM) detection. In this study, we applied HRAM mass spectrometer-Q-Exactive (Thermo Scientific) to detect both polar metabolites and lipids.

Helminths are known to produce stage-specific metabolites [21]. Although both adult and infective stages of *N. brasiliensis* had many fatty acids in common, interestingly, 44 of the polar metabolites detected in the infective stage of *N. brasiliensis* were not detected in the ESP of their adult stage [21]. Such differences in the metabolic profiles could have resulted partially due to the different experimental conditions and analytical techniques used in two separate studies. Nevertheless, such marked differences in the metabolic profiles of two different life-cycle stages of *N. brasiliensis* suggest that there could be major metabolic changes accompanying the transition from one life-cycle stage to the next in parasitic helminths. Moreover, according to Barrett [96], there are variations in the distribution pattern and activity of enzymes and metabolite levels among the different developmental stages of helminths. For instance, adult and larval stages of *A. lumbricoides* and *S. mansoni* possess a marked difference in the isoenzyme patterns. When we compared metabolites identified from the somatic extracts of *N. brasiliensis* and *T. muris* infective stages, the percentage similarity for both polar and non-polar metabolites was quite low (34.5% and 18%, respectively) despite sharing some common metabolites such as L-citrulline, L-threonine, deoxyadenosine, and pyridoxal. Metabolites such as inosine, hypoxanthine, and L-pipecolate were comparatively higher in NB_SE and were also reported significantly in high levels in the blood plasma samples of patients suffering from onchocerciasis (caused by nematode *Onchocerca volvulus*) [97]. The lower percentage similarity of metabolites in the somatic extracts of the two helminths could have resulted from the different conditions they were exposed to, as *N. brasiliensis* L3 were incubated at 26 °C with activated charcoal and later at 37 °C, 5% CO_2 in glutamax/Phosphate-buffered saline (PBS) media. At the same time, *T. muris* eggs were kept in PBS at room temperature. Thus, suggesting that the different environmental niches in which they survive—for instance, the L3 of human hookworms *N. americanus* and *A. duodenale* remain outdoors, while their adult stage dwells inside the host gut [4]—could potentially influence the types as well

as the level of metabolites produced. However, the effects of CO_2 tensions and temperature on the overall metabolic pathways are either complex or difficult to predict [96].

More than half of the metabolites identified in all sample groups were amino acids. L-citrulline, L-methionine, N(pi)-Methyl-L-histidine, succinate, and 4-hydroxybenzoate were the top five most abundant metabolites (based on LC-MS peak intensity) in the somatic extract and excretory/secretory products of *N. brasiliensis* L3. Succinate, one of the amino acids detected in the current study samples, is known to be produced by the intestinal microbiota to induce intestinal tufT cells to trigger T-helper cell type 2 (T_H2) responses [98]. Somatic and ESP of the adult stage of *N. brasiliensis* also contained succinate [21]. In the *T. muris* embryonated eggs, L-2-aminoadepate, N-acetylputrescine, L-pipecolate, thymine, and maleic acid were present in the highest intensities. Betaine is another amino acid detected in the infective stage of *N. brasiliensis* but not in their adult stage [21]. Betaine (a derivative of amino acid glycine with three methyl groups), present in microorganisms, plants and animals, is known to function as an osmolyte in their cells [99]. The plasma and spleen of rats infected with the liver fluke *Fasciola hepatica* also contained a high level of betaine [100]. Another metabolite that was prominent in both *N. brasiliensis* L3 ESP and *T. muris* embryonated eggs was L-glutamate. The dormant infective eggs of other helminths such as *A. lumbricoides* also contained L-glutamate [101]. The relevance of betaine and L-glutamate (and glutamine) in this study should be interpreted with caution, as it is possible that samples were contaminated by the sulfobetaine polymer (PSB) used for the somatic extract preparation and the glutamax used in the media. Pyroglutamic acid (also called 5-oxoproline), reported as one of the major metabolites in the somatic extracts of the adult stage of *N. brasiliensis* and *T. muris* [21], was a common metabolite in the infective stages of two helminths. Somatic extract of adult *Ancylostoma caninum* (dog hookworm) also contained pyroglutamic acid as one of the major metabolite constituents [102]. Pyroglutamic acid is formed as an intermediate product by the enzyme γ-glutamylcyclotransferase in glutathione metabolism, and it is ultimately converted into L-glutamic acid by 5-oxoprolinase [103]. It is also known to be produced due to disordered glutathione metabolism [104] and usually tends to accumulate abnormally in the case of metabolic acidosis.

Another exciting difference among the samples from two helminths is the presence of unique metabolites. Seven polar metabolites, namely orotate, pterin, 2,5-dihydroxybenzoate, LL-2,6-Diaminoheptanedioate, isocitrate, 5-oxoproline, and homogentisate, were found unique to the ESP of *N. brasiliensis*. Out of these seven, only isocitrate and 5-oxoproline were reported in their adult ESP [21]. In mammals, orotate (orotic acid) is released by mitochondrial dihydroorotate dehydrogenase for conversion to uridine monophosphate during pyrimidine metabolism [105]. Moreover, five main enzymes involved in pyrimidine metabolism are present in many helminths, including *N. brasiliensis* and *T. muris* [106], indicating that de novo pyrimidine biosynthesis could be the main source of orotate in helminths. Pterins are found in all living organisms starting from tiny bacteria to mammals and serve as a urine biomarker for hyperphenylalaninaemia [107]. Homogentisate is the central intermediate product in the catabolism of phenylalanine and tyrosine [108]. Whilst we have not ruled out the possibility that this feature could be another isomer of dihydroxyphenylacetate, it is most likely an intermediate in tyrosine/phenylalanine metabolism. Tyrosine catabolism is considered as a critical metabolic pathway in *Rhodnius prolixus*, a blood-sucking insect vector of *Trypanosoma cruzi*, because *R. prolixus* dies after a blood meal if the pathway is disturbed by silencing two critical enzymes, tyrosine aminotransferase and 4-hydroxyphenylpyruvate dioxygenase [109]. Thus, the presence of phenylalanine and tyrosine in *N. brasiliensis* L3 ESP could mean that tyrosine catabolism may be important for the survival of *N. brasiliensis* L3 when establishing a successful infection. Homogentisate also possesses antioxidant activity higher than α-tocopherol and moderate anti-inflammatory activity [110]. Thus, the capacity of ESP from many helminths, including *N. brasiliensis*, to reduce T-cell proliferation [111] and confer protection against T-cell mediated immunopathology in a mouse model of colitis [102], are attributable to the presence of such metabolites.

Identifying different metabolic pathways within a species is considered necessary, mainly to understand any malfunctions or alterations that may occur during disease state [112]. Similarly,

identifying metabolic pathways in soil-transmitted helminths might reveal a unique metabolic pathway(s) critical in the infection process and, therefore, present as drug targets. The metabolic pathway analysis revealed that the majority of the metabolic pathways are associated with amino acid metabolism, a finding that aligns with earlier metabolic profiling of the ESP from adult stage STHs [21], suggesting that both the infective and adult stages share similar (amino acid and carbohydrate) metabolic pathways. Polar metabolites identified from the infective stages of both helminths mostly belonged to common amino acid pathways such as aminoacyl-tRNA biosynthesis, arginine biosynthesis, lysine degradation, alanine, aspartate, and glutamate metabolism. Amino acids, such as leucine, lysine, and phenylalanine, are detected significantly in high concentrations in the herbivorous youngstock acutely infected with helminths [113]. L-arginine is known to enhance intestinal mucosa function by reducing tissue damage in intestinal ischemia of animal models [114,115]. We also found purine, glyoxylate, and dicarboxylate metabolism as major pathways following amino acid pathways. Glyoxylate metabolism, which is characteristic of free-living parasitic nematodes (but not in the adult) and catalyses the conversion of lipids into carbohydrates [96], could be the source of isocitrate (organic acid), which was one of the unique metabolites in the *N. brasiliensis* ESP.

Lipids and fatty acids are also known to play a crucial role in the maturation and completion of different life-cycle stages of helminths and host–parasite interaction [23]. Generally, the parasitic stage of helminths utilise lipids for the long-term adaptation inside their host and completion of the life-cycle [116]. Lipids are also involved in essential biological processes such as apoptosis, cell proliferation, angiogenesis, immunity, and inflammation [117]. Fatty acids, including the *cis*-form of octadecenoic acid and other branched-chain and monoenoic acids (oleic acids and vaccenic acid), are known to play a vital role in helminth infections by altering the physical properties of the host cell membrane and ultimately causing it to rupture [118]. Thus, we presume that fatty acids, such as octadecanoic acid detected in the ESP of *N. brasiliensis* L3, might be playing a key role during the process of host invasion and infection. Fatty acids were also reported in other nematodes such as *Haemonchus contortus* (in all stages of life-cycle) [119] and adult *Caenorhabditis elegans* [120], and in both studies, fatty acids with 18 carbons (i.e., 18:1, 18:2, and 18:3) were commonest. We also obtained a similar result, where ~7% of total lipids were fatty acids, and the above-mentioned fatty acids with 18 carbons were present in all three samples (i.e., NB_SE, NB_ESP, and TM_SE). Nematodes regulate the saturation levels of fatty acids while adapting to the changing environmental temperature [121], but the saturation level varies among different nematodes. For example, in *C. elegans*, the saturated fatty acid level increases with increasing temperature [122]. In contrast, Wang et al. [119] observed the opposite in *H. contortus*, where the level of fatty acid saturation tended to decrease as they transitioned from their free-living stage to the parasitic stage.

Glycerophospholipids and glycerolipids were the major lipid groups in all three sample groups (NB_SE, NB_ESP, and TM_SE), constituting approximately 83% of the total lipids. This is in congruence with lipidomic studies in the muscle-stage larvae of *Trichinella papuae* (~63% glycerophospholipids) [123] and in the *H. contortus* (all life-cycle stages), where more than 90% of the total lipids were glycerophospholipids and glycerolipids [119]. The somatic extract of *N. brasiliensis* L3 contained elements of glycerophospholipids such as phosphatidylcholine, PC(38:6), PC(40:8), PC(40:7), PC(40:9), and PC(46:5). Wewer et al. [124] also reported PC as dominant lipid constituents in filarial nematodes *Onchocerca volvulus*, *O. ochengi,* and *Litomosoides sigmodontis* but they have studied only their adult stage. Meanwhile, glycerolpids such as TG(45:0), TG(48:1), TG(50:2), TG(30:0), TG(38:0), and TG(38:1) were dominant in the excretory/secretory product of *N. brasiliensis* L3 and somatic extract of *T. muris* embryonated eggs. TG constituted major lipids (80.9% of total 327 lipids) identified from the somatic extract of the L3 stage of *H. contortus* and it decreases as they mature into L4 stage [119]. Lee [125] also reported triglycerides as a major lipid constituent in the adult tissue of *N. brasiliensis*, which was presumed to be due to reduced lipid metabolism under anaerobic conditions inside their host. Triglyceride is the major neutral lipid in the majority of helminths [126]. According to Ward [118], unlike mammals, helminths are capable of storing a large amount of energy in the form of glycerolipids

as triglycerides or triacylglycerides have more energy content (9 kcal/g) compared to carbohydrates (4 kcal/g). Thus, it is likely that infective stages of both helminths *N. brasiliensis* L3 and *T. muris* embryonated eggs store energy in the form of triglycerides for their later developmental stages of the life-cycle. Our findings complement a similar study where the *Schistosoma mansoni* infective stage (cercariae) had a unique lipid profile compared to other stages of the life-cycle [23]. Interestingly, although *S. mansoni* belongs to a different phylum (Platyhelminthes), it shares some behavioural aspects with *N. brasiliensis*—notably, the penetration of host skin by the infective stage larvae. Although we could not retrieve literature on pharmacological activities of specific triglycerides identified in this study, a high level of triglycerides was associated with inflammation and inflammation-related disorders [127]. *T. muris* embryonated eggs showed enrichment of species of phosphatidic acids (PA), out of which PA(25:0) and PA(26:0) were completely absent in the infective stage L3 of *N. brasiliensis*. Phosphatidic acid is a lipid of interest as a vital signalling molecule and a central intermediate in the synthesis of membrane lipids and storage lipids [128,129]. Phosphatidic acid, such as lysoPA (C14:2), was also detected in the surface coat of the infective stage of the parasitic nematode *Trichinella spiralis* [130]. Other species of helminths such as *Hymenolepis diminuta*, *A. lumbricoides*, *Dirofilaria immitis*, and *Setaria cervi* also contained phosphatidic acids [126]. Phosphatidylcholines (PC) reported to be produced by all life-cycle stages of parasitic trematode [23] were also detected in both helminths studied here. PC lipids are associated with the maintenance of gastrointestinal mucus barrier function [131], besides their good anti-inflammatory properties [132,133]. PC lipids such as PC(36:7), PC(P-32:2), and PC(P-36:2) were unique to *N. brasiliensis* L3 somatic extract.

4. Materials and Methods

4.1. Ethics, Source, and Housing of Mice and Rats

Mice strain B10.Br (5 weeks old, 5 mice per cage) and rat strain Sprague–Dawley (2 weeks old, 2 rats per cage) were purchased from Animal Resources Centre (Perth, Australia). All experiments using these animals were approved by the animal ethics committee of James Cook University (JCU), Cairns, Australia (animal ethics number: A2647). Mice and rats were kept in the JCU animal facility centre in compliance with JCU approved protocols, Australian Code of Practice for the Care and Use of Animals for Scientific Purposes, (7th edition, 2007), and the Queensland Animal Care and Protection Act 2001. The animal facility room had an ambient temperature (20–22 °C) and humidity (60%), and animals were exposed to a 12 h day/night cycle and fed irradiated mouse/rat chow (Specialty Feeds, Glen Forrest, Western Australia) and autoclaved tap water ad libitum.

4.2. Collection of N. brasiliensis L3 and Its ESP

Sprague–Dawley rats were infected with *N. brasiliensis* L3 (~3000 larvae) by subcutaneous injection and sacrificed on day seven post-infection [134]. We collected faecal pellets on day five and six post-infection. Subsequently, faecal pellets were cultured with activated charcoal—untreated, granular, 8–20 mesh (Sigma-Aldrich, New South Wales, Australia). The culture plates were sealed inside an airtight plastic container in an incubator (Binder, model: BD 115 #02-040007) at 26 °C for one week. After one-week incubation, L3 were harvested, washed with warmed 5× pen/strep PBS, and then transferred to a 12-well culture plate (1500 worms per well) containing warmed 2 mL 5× glutamax, 2× pen/strep PBS media. Plates were incubated in a CO_2 incubator (Sanyo MCO-18AIC CO_2 incubator, SANYO Electric Co., Ltd., Moriguchi, Japan) at 37 °C supplied with 5% CO_2. The supernatant (ESP) was collected and replaced with fresh media twice daily (09:00 and 17:00) for four consecutive days. The supernatants were centrifuged at 3000× *g* for 30 min, and then aliquot was transferred to Amicon® Ultra-15, centrifugal 10 kDa filters (Merck Millipore, Victoria, Australia), and centrifuged at 4000× *g* for 20 min. Concentrated ESP filtrate containing small molecules (<10 kDa) was collected and stored at −80 °C until further analysis.

4.3. Collection of Eggs (Infective Stage) from T. muris Adult Worms

B10.Br mice were infected with *T. muris* embryonated eggs (200 µL of PBS containing ~200 eggs) through oral gavage. We euthanised mice with CO_2 on day 30–33 post-infection to harvest adult *T. muris* for egg collection. Caecum was collected, split longitudinally, and washed in warmed 5× pen/strep in PBS. Adult worms were carefully pulled from the caecum of mice with fine forceps and washed with 5x pen/strep in PBS, and then transferred to 6-well culture plates (~100 worms per well) containing 4 mL of warmed 5× glutamax, 2× pen/strep in PBS media. Worms were incubated in a CO_2 incubator at 37 °C in 5% CO_2. For egg collection, we replaced culture media with fresh media twice daily as described above for three consecutive days. The supernatant was collected twice daily and centrifuged at 3000× *g* for 30 min. Eggs from adult *T. muris* worms were resuspended in 40 mL milli-Q water and filtered through a 100 µm nylon sieve before transferring to a fresh cell culture tube. Finally, for eggs to become embryonated, eggs were kept in the sterile PBS and stored in the dark at room temperature for approximately six weeks, and then stored at 4 °C.

4.4. Somatic Extract Preparation

Somatic extracts of *N. brasiliensis* L3 (five biological replicates named as NB_SE_1, NB_SE_2, NB_SE_3, NB_SE_4, and NB_SE_5, each replicate containing ~17000 L3) and *T. muris* embryonated eggs (five biological replicates named as TM_SE_1, TM_SE_2, TM_SE_3, TM_SE_4, and TM_SE_5, each replicate containing ~17000 eggs) were suspended in 1 mL chilled sulfobetaine polymer (PSB) and centrifuged at 1000× *g* for 5 min at 4 °C. The supernatant was discarded, and the remaining solid was resuspended in 250 µL of chilled extraction solvent ($CHCl_3$:MeOH:H_2O, 1:3:1, *v*/*v*) containing 1 µM of internal standards 3-(cyclohexyl amino)-1-propane sulfonic acid (CAPS), 3-[(3-cholamidopropyl) dimethylammonio]-1-propanesulphonate (CHAPS), piperazine-N,N′-bis(2-ethane sulfonic acid (PIPES), and Tris(hydroxylmethyl)amino-methane (Tris). A blank sample containing water instead of a tissue pellet was extracted simultaneously as a control. After three freeze–thaw cycles, the samples were mixed thoroughly for 30 min at 4 °C. The samples were centrifuged at 14,800× *g* for 10 min at 4 °C. Supernatant (100 µL) was transferred to the vials for metabolomics analysis and analysed on the same day. Another 100 µL was transferred to microfuge tubes for lipidomics analysis. The solvent was evaporated using a centrifugal evaporator at 55 °C for 50 min. Dried extracts were frozen at −80 °C until LC-MS analysis was performed. On the day of analysis, the samples were dissolved in 80 µL of BuOH:MeOH:H_2O (4.5:4.5:1, *v*/*v*). The samples were shaken for 30 min at room temperature and sonicated for 1 h while maintaining the temperature below 25 °C. The samples were centrifuged at 14,800× *g* for 10 min at 20 °C, and then 70 µL was transferred to LC-MS vials.

4.5. ESP Extract Preparation

ESP from *N. brasiliensis* L3 was thawed on ice and 100 µL aliquots of ESP (five biological replicates named as NB_ESP_1, NB_ESP_2, NB_ESP_3, NB_ESP_4, and NB_ESP_5) were transferred to microfuge tubes kept on ice. Subsequently, 400 µL of extraction solvent ($CHCl_3$:MeOH, 1:3, *v*/*v*) containing 1 µM of internal standards CAPS, CHAPS, and PIPES was added to each replicate. The mixture was shaken at 4 °C for 30 min and centrifuged at 14,800× *g* for 10 min at 4 °C. Then, 100 µL of supernatant was transferred to the vials for metabolomic analysis and 10 µL was combined to make a pooled quality control (QC) sample.

For the lipidomics analysis, 240 µL of supernatant was transferred to microfuge tubes and evaporated at 20 °C under a stream of nitrogen and stored at −80 °C. On the day of analysis, the samples were dissolved in 80 µL of BuOH/MeOH/H_2O (4.5:4.5:1, *v*/*v*), shaken for 30 min at room temperature, and sonicated for 1 h, keeping the temperature below 25 °C. The samples were centrifuged at 14,800× *g* for 10 min at 20 °C and then 70 µL of the sample was transferred to LC-MS vials and the leftover was combined to make a pooled QC sample.

4.6. Metabolomics LC-MS Data Acquisition

LC-MS data were acquired on a Q-Exactive Orbitrap mass spectrometer (Thermo Fischer Scientific, Waltham, MA, USA) coupled with high-performance liquid chromatography (HPLC) system Dionex Ultimate® 3000 RS (Thermo Scientific, Waltham, MA, USA) [135] as outlined in the Figure 1. The samples were analysed as a single batch to avoid batch-to-batch variation and randomised to account for the LC-MS system drift over time. Chromatographic separation was performed on ZIC-pHILIC column (5 µm, 4.6 × 150 mm, SeQuant®, Merck) (Merck Millipore, Victoria, Australia) equipped with a guard (ZIC-pHILIC). The mobile phase (A) was 20 mM ammonium carbonate (Sigma Aldrich, New South Wales, Australia), and (B) acetonitrile (Thermo Fischer Scientific, Melbourne, Australia). The needle wash solution was 50% isopropanol. The gradient program started at 80% B and was decreased to 50% B over 15 min, then to 5% B until 18 min, kept at 5% B until 21 min, returned to 80% B by 24 min, and equilibrated at 80% B to 32 min. The flow rate was 0.3 mL.min^{-1} and column compartment temperature was 25 °C. The total run time was 32 min, with an injection volume of 10 µL. The mass spectrometer was operated in full scan mode with positive and negative polarity switching at 35 k resolution at 200 *m*/*z* with a detection range of 85 to 1275 *m*/*z*, AGC target 1×10^6 ions, maximum injection time 50 ms. Heated electro-spray ionisation source (HESI) was set to 4.0 kV voltage for positive and negative mode, and sheath gas was set to 50, aux gas to 20, and sweep gas to 2 arbitrary units (AU), capillary temperature was 300 °C, and probe heater temperature was 120 °C.

4.7. Lipidomics LC-MS Data Acquisition

Chromatographic separation was performed on an Agilent Zorbax C8 (1.8 µm, 2.1 × 100 mm, Agilent Technologies, Victoria, Australia) equipped with a guard column (C8, 2 × 2 mm, Phenomenex, New South Wales, Australia) [136]. The mobile phase (A) was 40% isopropanol, 8 mM ammonium formate, and 2 mM formic acid, and (B) 98% isopropanol, 8 mM ammonium formate and 2 mM formic acid, and needle wash solution was 50% isopropanol. The gradient program started at 0% B and was increased stepwise to 20% B over 1.5 min, to 28% B over 5.5 min, to 35% B over 1 min, to 65% B over 16 min, and 100% B over 1 min. Wash at 100% B was continued for 2 min before decreasing to 0% B over the next 2 min, followed by equilibration at 0% B for 1 min. The flow rate was 0.2 mL.min^{-1} and column compartment temperature was 40 °C. The total run time was 30 min, with an injection volume of 10 µL. The mass spectrometer was operated in full scan mode with positive and negative polarity switching at 70 k resolution at 200 *m*/*z* with a detection range of 140 to 1300 *m*/*z*, AGC target 1×10^6 ions, maximum injection time 50 ms. Heated electro-spray ionisation source (HESI) was set to 3.5 kV for both positive mode and negative modes, and sheath gas was set to 34 AU, auxiliary gas to 13 AU, and sweep gas to 1 AU. Capillary and probe heater temperatures were set to 250 and 190 °C, respectively.

4.8. Data Processing Using IDEOM

The acquired LC-MS data were processed in untargeted fashion using open source software IDEOM [137], which was initially used ProteoWizard to convert raw LC-MS files to mzXML format and XCMS to pick peaks. Mzmatch.R was used to convert to peakML files [138], and for sample alignment and the filtering of peaks using a minimum detectable intensity of 100,000, relative standard deviation (RSD) of <0.5 (reproducibility), and peak shape (codadw) of >0.8. Mzmatch was also used to retrieve missing peaks and annotate related peaks. Default IDEOM parameters were used to eliminate unwanted noise and artefact peaks. The loss or gain of a proton was corrected in negative and positive ESI mode, respectively, followed by putative identification of metabolites by accurate mass within 3 ppm mass error by searching against the Kyoto Encyclopedia of Genes and Genomes (KEGG), MetaCyc, and LIPIDMAPS databases. Additional manual curation was performed to remove putative lipids that did not elute at the expected retention time.

4.9. Data Analyses and Statistical Interpretation

We performed chemometric univariate and multivariate statistical analyses using the Metaboanalyst website (http://www.metaboanalyst.ca) [139]. Before chemometric univariate and multivariate statistical analyses, data integrity was checked and filtered to ensure all data had been included. The sample data (spectral data) were normalised, log transformed, and auto-scaled before analysis. For univariate analysis, volcano plot analysis was performed to identify differential metabolites using the t-test and fold-change (FC) methods, and plots log2 (fold-change > 2) on the *X*-axis against −log10 (*p*-value) from the t-test on the *Y*-axis. Benjamini–Hochberg correction or false discovery rate (FDR) was applied to compute the number of false positives out of significantly varied metabolic features.

In multivariate analyses, we performed principal component analysis (PCA) unsupervised method and hierarchical clustering analysis (HCA) with Euclidean measured distance, and the ward.D clustering algorithm was used to evaluate the difference in the concentration of each metabolite between sample groups.

Before the pathway analysis, IDs for the metabolites were obtained from the KEGG, LipidMAPS, PubChem Compound ID (PubChem CID), Human Metabolome Database (HMDB), and the Chemical Translation service (CTS; https://cts.fiehnlab.ucdavis.edu). Subsequently, we performed pathway enrichment analysis using the Metaboanalyst website (http://www.metaboanalyst.ca) [139].

4.10. Literature Review on Pharmacological Properties of Identified Metabolites

We conducted a comprehensive literature search for the pharmacological properties of metabolites identified in this study using various search engines, including PubMed, Medline, Google Scholar, and SciFinder Scholar. Keywords such as "anti-inflammatory," "bioactivity," "pharmacological activity," and "anti-oxidant activity" were used to identify reported pharmacological activities of metabolites.

5. Conclusions

In summary, we show that the infective stages of two different STHs produce characteristic metabolites. The current study identified many unique metabolites (both polar as well as non-polar metabolites) present in the infective stages of *N. brasiliensis* (seven unique polar metabolites and 28 lipids in the somatic extract) and *T. muris* eggs (four unique lipids). Future studies should further characterise their identity and bioactivity in more detail. The vast array of metabolites identified from these two helminths' infective stages could potentially serve as a database for the in-depth understanding of helminth biochemistry, which is currently lacking. Moreover, the suite of metabolites identified in this study presents a potential avenue for future research, particularly for the development of metabolite-based diagnosis tools and the identification of novel targets for anthelmintic drugs.

Supplementary Materials: The following are available online at http://www.mdpi.com/2218-1989/10/11/446/s1, Table S1: Total putative polar metabolites identified in the infective stages of *Nippostrongylus brasiliensis* and *Trichuris muris*, Table S2: Total putative lipids identified in the infective stages of *Nippostrongylus brasiliensis* and *Trichuris muris*, Table S3: Fold change analysis of putative lipids between the infective stage of *N. brasiliensis* somatic extract (NB_SE) and *T. muris* embryonated egg extract (TM_SE).

Author Contributions: Conceptualisation, P.W. and A.L.; methodology, P.W., L.B. and K.Y.; software, D.A., K.Y. and P.W.; validation, D.J.C. and D.A.; formal analysis, D.A., D.J.C., K.Y. and P.W.; investigation, D.A. and D.J.C.; resources, A.L., and P.W.; data curation, D.A., and D.J.C.; writing—original draft preparation, K.Y.; writing—review and editing, P.W., A.L., L.B., E.R. and D.J.C.; visualisation, P.W.; supervision, P.W. and A.L.; project administration, P.W.; funding acquisition, A.L. and P.W. All authors have read and agreed to the published version of the manuscript.

Funding: This work was funded by a James Cook University Postgraduate Research Scholarship (JCUPRS) to K.Y.; a National Health and Medical Research Council (NHMRC) Ideas Grant (APP1183323) to P.W., an Australian Institute of Tropical Health and Medicine Capacity Development Grant to P.W.; an NHMRC Program Grant (APP1132975) to A.L., and a Senior Principal Research Fellowship (APP1117504) to A.L.

Conflicts of Interest: All authors declare that there are no conflicts of interest.

References

1. WHO. *Investing to Overcome the Global Impact of Neglected Tropical Diseases: Third WHO Report on Neglected Tropical Diseases 2015*; World Health Organization: Geneva, Switzerland, 2015; pp. 1–191.
2. Hotez, P.J.; Brindley, P.J.; Bethony, J.M.; King, C.H.; Pearce, E.J.; Jacobson, J. Helminth infections: The great neglected tropical diseases. *J. Clin. Investig.* **2008**, *118*, 1311–1321. [CrossRef] [PubMed]
3. WHO. *Soil-Transmitted Helminth Infections*; World Health Organization: Geneva, Switzerland, 2019.
4. Brooker, S.; Bethony, J.; Hotez, P.J. Human Hookworm Infection in the 21st Century. *Adv. Parasitol.* **2004**, *58*, 197–288. [PubMed]
5. Bethony, J.; Brooker, S.; Albonico, M.; Geiger, S.M.; Loukas, A.; Diemert, D.; Hotez, P.J. Soil-transmitted helminth infections: Ascariasis, trichuriasis, and hookworm. *Lancet* **2006**, *367*, 1521–1532. [CrossRef]
6. Dunn, J.C.; Bettis, A.A.; Wyine, N.Y.; Lwin, A.M.M.; Tun, A.; Maung, N.S.; Anderson, R.M. Soil-transmitted helminth reinfection four and six months after mass drug administration: Results from the delta region of Myanmar. *PLoS Negl. Trop. Dis.* **2019**, *13*, 1–16. [CrossRef] [PubMed]
7. Tchuem Tchuente, L.A. Control of soil-transmitted helminths in sub-Saharan Africa: Diagnosis, drug efficacy concerns and challenges. *Acta. Trop.* **2011**, *120S*, S4–S11. [CrossRef] [PubMed]
8. Holden-Dye, L.; Walker, R.J. Anthelmintic drugs. *WormBook Ed. C Elegans Res. Community WormBook* **2007**, 1–13. [CrossRef]
9. Ok, K.S.; Kim, Y.S.; Song, J.H.; Lee, J.H.; Ryu, S.H.; Lee, J.H.; Moon, J.S.; Whang, D.H.; Lee, H.K. Trichuris trichiura infection diagnosed by colonoscopy: Case reports and review of literature. *Korean J. Parasitol.* **2009**, *47*, 275–280. [CrossRef]
10. Easton, A.V.; Oliveira, R.G.; O'Connell, E.M.; Kepha, S.; Mwandawiro, C.S.; Njenga, S.M.; Kihara, J.H.; Mwatele, C.; Odiere, M.R.; Brooker, S.J.; et al. Multi-parallel qPCR provides increased sensitivity and diagnostic breadth for gastrointestinal parasites of humans: Field-based inferences on the impact of mass deworming. *Parasit Vectors* **2016**, *9*, 38. [CrossRef]
11. WHO. *Prevention and Control of Schistosomiasis and Soil-Transmitted Helminthiasis: Report of a WHO Expert Committee*; World Health Organization: Geneva, Switzerland, 2002.
12. Knopp, S.; Rinaldi, L.; Khamis, I.S.; Stothard, J.R.; Rollinson, D.; Maurelli, M.P.; Steinmann, P.; Marti, H.; Cringoli, G.; Utzinger, J. A single FLOTAC is more sensitive than triplicate Kato-Katz for the diagnosis of low-intensity soil-transmitted helminth infections. *Trans. R. Soc. Trop. Med. Hyg.* **2009**, *103*, 347–354. [CrossRef]
13. Coghlan, A.; Tygai, R.; Cotton, J.A. Comparative genomics of the major parasitic worms. *Nat. Genet.* **2018**, 163–174. [CrossRef]
14. Jex, A.R.; Waeschenbach, A.; Hu, M.; van Wyk, J.A.; Beveridge, I.; Littlewood, D.T.; Gasser, R.B. The mitochondrial genomes of Ancylostoma caninum and Bunostomum phlebotomum—Two hookworms of animal health and zoonotic importance. *BMC Genom.* **2009**, *10*, 1–10. [CrossRef]
15. Meekums, H.; Hawash, M.B.; Sparks, A.M.; Oviedo, Y.; Sandoval, C.; Chico, M.E.; Stothard, J.R.; Cooper, P.J.; Nejsum, P.; Betson, M. A genetic analysis of Trichuris trichiura and Trichuris suis from Ecuador. *Parasit. Vectors* **2015**, *8*, 1–5. [CrossRef] [PubMed]
16. Tang, Y.T.; Gao, X.; Rosa, B.A.; Abubucker, S.; Hallsworth-Pepin, K.; Martin, J.; Tyagi, R.; Heizer, E.; Zhang, X.; Bhonagiri-Palsikar, V.; et al. Genome of the human hookworm Necator americanus. *Nat. Genet.* **2014**, *46*, 261–269. [CrossRef]
17. Foth, B.J.; Tsai, I.J.; Reid, A.J.; Bancroft, A.J.; Nichol, S.; Tracey, A.; Holroyd, N.; Cotton, J.A.; Stanley, E.J.; Zarowiecki, M.; et al. Whipworm genome and dual-species transcriptome analyses provide molecular insights into an intimate host-parasite interaction. *Nat. Genet.* **2014**, *46*, 693–700. [CrossRef]
18. Leroux, L.P.; Nasr, M.; Valanparambil, R.; Tam, M.; Rosa, B.A.; Siciliani, E.; Hill, D.E.; Zarlenga, D.S.; Jaramillo, M.; Weinstock, J.V.; et al. Analysis of the Trichuris suis excretory/secretory proteins as a function of life cycle stage and their immunomodulatory properties. *Sci. Rep.* **2018**, *8*, 1–17. [CrossRef]
19. Mulvenna, J.; Hamilton, B.; Nagaraj, S.H.; Smyth, D.; Loukas, A.; Gorman, J.J. Proteomics analysis of the excretory/secretory component of the blood-feeding stage of the hookworm, Ancylostoma caninum. *Mol. Cell Proteom.* **2009**, *8*, 109–121. [CrossRef]
20. Santos, L.N.; Gallo, M.B.; Silva, E.S.; Figueiredo, C.A.; Cooper, P.J.; Barreto, M.L.; Loureiro, S.; Pontes-de-Carvalho, L.C.; Alcantara-Neves, N.M. A proteomic approach to identify proteins from Trichuris trichiura extract with immunomodulatory effects. *Parasite Immunol.* **2013**, *35*, 188–193. [CrossRef]

21. Wangchuk, P.; Kouremenos, K.; Eichenberger, R.M.; Pearson, M.; Susianto, A.; Wishart, D.S.; McConville, M.J.; Loukas, A. Metabolomic profiling of the excretory-secretory products of hookworm and whipworm. *Metabolomics* **2019**, *15*, 1–15. [CrossRef] [PubMed]
22. Wangchuk, P.; Constantinoiu, C.; Eichenberger, R.M.; Field, M.; Loukas, A. Characterization of tapeworm metabolites and their reported biological activities. *Molecules* **2019**, *24*, 1480. [CrossRef] [PubMed]
23. Giera, M.; Kaisar, M.M.M.; Derks, R.J.E.; Steenvoorden, E.; Kruize, Y.C.M.; Hokke, C.H.; Yazdanbakhsh, M.; Everts, B. The Schistosoma mansoni lipidome: Leads for immunomodulation. *Anal. Chim. Acta* **2018**, *1037*, 107–118. [CrossRef] [PubMed]
24. Eichenberger, R.M.; Ryan, S.; Jones, L.; Buitrago, G.; Polster, R.; Montes de Oca, M.; Zuvelek, J.; Giacomin, P.R.; Dent, L.A.; Engwerda, C.R.; et al. Hookworm secreted extracellular vesicles interact with hosT cells and prevent inducible Colitis in mice. *Front. Immunol.* **2018**, *9*, 1–14. [CrossRef]
25. Eichenberger, R.M.; Talukder, M.H.; Field, M.A.; Wangchuk, P.; Giacomin, P.; Loukas, A.; Sotillo, J. Characterization of Trichuris muris secreted proteins and extracellular vesicles provides new insights into host-parasite communication. *J. Extracell. Vesicles* **2018**, *7*, 1–16. [CrossRef] [PubMed]
26. Drake, L.; Korchev, Y.; Bashford, L.; Djamgoz, M.; Wakelin, D.; Ashall, F.; Bundy, D. The major secreted product of the whipworm, *Trichuris*, is a pore-forming protein. *Prec. R. Soc. Lond. B* **1994**, *257*, 255–261.
27. Bancroft, A.J.; Levy, C.W.; Jowitt, T.A.; Hayes, K.S.; Thompson, S.; McKenzie, E.A.; Ball, M.D.; Dubaissi, E.; France, A.P.; Bellina, B.; et al. The major secreted protein of the whipworm parasite tethers to matrix and inhibits interleukin-13 function. *Nat. Commun.* **2019**, *10*, 2344. [CrossRef]
28. Williamson, A.L.; Brindley, P.J.; Knox, D.P.; Hotez, P.J.; Loukas, A. Digestive proteases of blood-feeding nematodes. *Trends Parasitol.* **2003**, *19*, 417–423. [CrossRef]
29. Stassens, P.; Bergum, P.W.; Gansemans, Y.; Jespers, L.; Laroche, Y.; Huang, S.; Maki, S.; Messens, J.; Lauwereys, M.; Cappello, M.; et al. Anticoagulant repertoire of the hookworm Ancylostoma caninum. *Proc. Natl. Acad. Sci. USA* **1996**, *93*, 2149–2154. [CrossRef] [PubMed]
30. Navarro, S.; Pickering, D.A.; Ferreira, I.B.; Jones, L.R.S.; Troy, S.; Leech, A.; Hotez, P.J.; Zhan, B.; Laha, T.P.R.; Sparwasser, T.; et al. Hookworm recombinant protein promotes regulatory T cell responses that suppress experimental asthma. *Sci. Transl. Med.* **2016**, *8*, 1–14. [CrossRef]
31. Shepherd, C.; Navarro, S.; Wangchuk, P.; Wilson, D.; Daly, N.L.; Loukas, A. Identifying the immunomodulatory components of helminths. *Parasite Immunol.* **2015**, *37*, 293–303. [CrossRef] [PubMed]
32. Fukuda, T.; Majumder, K.; Zhang, H.; Matsui, T.; Mine, Y. Adenine has an anti-inflammatory effect through the activation of adenine receptor signaling in mouse macrophage. *J. Funct. Foods* **2017**, *28*, 235–239. [CrossRef]
33. Yang, D.; Zhang, Y.; Nguyen, H.G.; Koupenova, M.; Chauhan, A.K.; Makitalo, M.; Jones, M.R.; St Hilaire, C.; Seldin, D.C.; Toselli, P.; et al. The A2B adenosine receptor protects against inflammation and excessive vascular adhesion. *J. Clin. Investig.* **2006**, *116*, 1913–1923. [CrossRef]
34. Hasko, G.; Kuhel, D.G.; Nemeth, Z.H.; Mabley, J.G.; Stachlewitz, R.F.; Virag, L.; Lohinai, Z.; Southan, G.J.; Salzman, A.L.; Szabo, C. Inosine inhibits inflammatory cytokine production by a posttranscriptional mechanism and protects against endotoxin-induced shock. *J. Immunol.* **2000**, *164*, 1013–1019. [CrossRef]
35. Liaudet, L.; Mabley, J.G.; Soriano, F.G.; Pacher, P.; Marton, A.; Hasko, G.; Szabo, C. Inosine reduces systemic inflammation and improves survival in septic shock induced by cecal ligation and puncture. *Am. J. Respir. Crit. Care Med.* **2001**, *164*, 1213–1220. [CrossRef]
36. Lee, B.J.; Lin, J.S.; Lin, Y.C.; Lin, P.T. Antiinflammatory effects of L-carnitine supplementation (1000 mg/d) in coronary artery disease patients. *Nutrition* **2015**, *31*, 475–479. [CrossRef]
37. Keskin, E.; Uluisik, D.; Altin, M. Antioxidant effect of L-carnitine in rats fed cholesterol rich diet. *Anim. Vet. Sci.* **2015**, *3*, 113–116. [CrossRef]
38. Detopoulou, P.; Panagiotakos, D.B.; Antonopoulou, S.; Pitsavos, C.; Stefanadis, C. Dietary choline and betaine intakes in relation to concentrations of inflammatory markers in healthy adults: The ATTICA study. *Am. J. Clin. Nutr.* **2008**, *87*, 424–430. [CrossRef]
39. Joshi, A.; Kimball, A.; Schaller, M.; denDekker, A.; Burant, C.; Kunkel, S.L.; Gallagher, K. Modulation of Xanthine metabolism ameliorates inflammation and accelerates diabetic wound healing. *J. Immunol.* **2018**, *200*, 170-13.
40. Afraei, S.; D'Aniello, A.; Sedaghat, R.; Ekhtiari, P.; Azizi, G.; Tabrizian, N.; Magliozzi, L.; Aghazadeh, Z.; Mirshafiey, A. Therapeutic effects of D-aspartate in a mouse model of multiple sclerosis. *J. Food. Drug. Anal.* **2017**, *25*, 699–708. [CrossRef]

41. Boccella, S.; Vacca, V.; Errico, F.; Marinelli, S.; Squillace, M.; Guida, F.; Di Maio, A.; Vitucci, D.; Palazzo, E.; De Novellis, V.; et al. D-aspartate modulates nociceptive-specific neuron activity and pain threshold in inflammatory and neuropathic pain condition in mice. *Biomed. Res. Int.* **2015**, *2015*, 1–10. [CrossRef]
42. Littlewood-Evans, A.; Sarret, S.; Apfel, V.; Loesle, P.; Dawson, J.; Zhang, J.; Muller, A.; Tigani, B.; Kneuer, R.; Patel, S.; et al. GPR91 senses extracellular succinate released from inflammatory macrophages and exacerbates rheumatoid arthritis. *J. Exp. Med.* **2016**, *213*, 1655–1662. [CrossRef]
43. Lei, W.; Ren, W.; Ohmoto, M.; Urban, J.F., Jr.; Matsumoto, I.; Margolskee, R.F.; Jiang, P. Activation of intestinal tuft cell-expressed Sucnr1 triggers type 2 immunity in the mouse small intestine. *Proc. Natl. Acad. Sci. USA* **2018**, *115*, 5552–5557. [CrossRef]
44. Fujino, M.; Nishio, Y.; Ito, H.; Tanaka, T.; Li, X.K. 5-Aminolevulinic acid regulates the inflammatory response and alloimmune reaction. *Int. Immunopharmacol.* **2016**, *37*, 71–78. [CrossRef]
45. Yamaguchi, H.; Maruyama, T.; Urade, Y.; Nagata, S. Immunosuppression via adenosine receptor activation by adenosine monophosphate released from apoptotic cells. *Elife* **2014**, *3*, 1–15. [CrossRef]
46. Sag, D.; Carling, D.; Stout, R.D.; Suttles, J. Adenosine 5′-monophosphate-activated protein kinase promotes macrophage polarization to an anti-inflammatory functional phenotype. *J. Immunol.* **2008**, *181*, 8633–8641. [CrossRef] [PubMed]
47. Lee, J.S.; Wang, R.X.; Alexeev, E.E.; Lanis, J.M.; Battista, K.D.; Glover, L.E.; Colgan, S.P. Hypoxanthine is a checkpoint stress metabolite in colonic epithelial energy modulation and barrier function. *J. Biol. Chem.* **2018**, *293*, 6039–6051. [CrossRef]
48. Jiao, N.; Wu, Z.; Ji, Y.; Wang, B.; Dai, Z.; Wu, G. L-Glutamate enhances barrier and antioxidative functions in intestinal porcine epithelial cells. *J. Nutr.* **2015**, *145*, 2258–2264. [CrossRef]
49. Unnikrishnan, M.K.; Rao, M.N.A. Antiinflammatory activity of methionine, methionine sulfoxide and methionine sulfone. *Agents Actions* **1990**, *31*, 110–112. [CrossRef]
50. Derakhshanfar, A.; Bidadkosh, A.; Hashempour Sadeghian, M. L-methionine attenuates gentamicin nephrotoxicity in male Wistar rat: Pathological and biochemical findings. *Iran. J. Vet. Res.* **2009**, *10*, 323–328.
51. Hasegawa, S.; Ichiyama, T.; Sonaka, I.; Ohsaki, A.; Okada, S.; Wakiguchi, H.; Kudo, K.; Kittaka, S.; Hara, M.; Furukawa, S. Cysteine, histidine and glycine exhibit anti-inflammatory effects in human coronary arterial endothelial cells. *Clin. Exp. Immunol.* **2012**, *167*, 269–274. [CrossRef]
52. Winter, A.N.; Brenner, M.C.; Punessen, N.; Snodgrass, M.; Byars, C.; Arora, Y.; Linseman, D.A. Comparison of the neuroprotective and anti-Inflammatory effects of the anthocyanin metabolites, protocatechuic acid and 4-hydroxybenzoic acid. *Oxid. Med. Cell Longev.* **2017**, *2017*, 1–13. [CrossRef]
53. Ullman, B.; Gudas, L.J.; Cohen, A.; Martin, D.W. Deoxyadenosine metabolism and cytotoxicity in cultured mouse T lymphoma cells: A model for immunodeficiency disease. *Cell* **1978**, *14*, 365–375. [CrossRef]
54. He, L.; Li, H.; Huang, N.; Zhou, X.; Tian, J.; Li, T.; Wu, J.; Tian, Y.; Yin, Y.; Yao, K. Alpha-ketoglutarate suppresses the NF-κB-mediated inflammatory pathway and enhances the PXR-regulated detoxification pathway. *Oncotarget* **2017**, *8*, 102974–102988. [CrossRef] [PubMed]
55. Velvizhi, S.; Nagalashmi, T.; Essa, M.M.; Dakshayani, K.B.; Subramanian, P. Effects of—Alpha-ketoglutarate on lipid peroxidation and antioxidant status during chronic ethnol administration in Wistar rats. *Pol. J. Pharmacol.* **2002**, *54*, 231–236. [PubMed]
56. Cavone, L.; Calosi, L.; Cinci, L.; Moroni, F.; Chiarugi, A. Topical mannitol reduces inflammatory edema in a rat model of arthritis. *Pharmacology* **2012**, *89*, 18–21. [CrossRef]
57. Naägeli, M.; Fasshauer, M.; Sommerfeld, J.; Fendel, A.; Brandi, G.; Stover, J.F. Prolonged continuous intravenous infusion of the dipeptide L-alanine- L-glutamine significantly increases plasma glutamine and alanine without elevating brain glutamate in patients with severe traumatic brain injury. *Nägeli Crit. Care* **2014**, *18*, 1–12. [CrossRef]
58. Coqueiro, A.Y.; Raizel, R.; Hypólito, T.M.; Tirapegui, J. Effects of supplementation with L-glutamine and L-alanine in the body composition of rats submitted to resistance exercise. *Rev. Bras. Cienc. Esporte* **2017**, *39*, 417–423. [CrossRef]
59. Raizel, R.; Leite, J.S.; Hypolito, T.M.; Coqueiro, A.Y.; Newsholme, P.; Cruzat, V.F.; Tirapegui, J. Determination of the anti-inflammatory and cytoprotective effects of l-glutamine and l-alanine, or dipeptide, supplementation in rats submitted to resistance exercise. *Br. J. Nutr.* **2016**, *116*, 470–479. [CrossRef] [PubMed]

60. Singhal, N.K.; Sternbach, S.; Fleming, S.; Alkhayer, K.; Shelestak, J.; Popescu, D.; Weaver, A.; Clements, R.; Wasek, B.; Bottiglieri, T.; et al. Betaine restores epigenetic control and supports neuronal mitochondria in the cuprizone mouse model of multiple sclerosis. *Epigenetics* **2020**, 1–16. [CrossRef]
61. Wu, J.; He, C.; Bu, J.; Luo, Y.; Yang, S.; Ye, C.; Yu, S.; He, B.; Yin, Y.; Yang, X. Betaine attenuates LPS-induced downregulation of Occludin and Claudin-1 and restores intestinal barrier function. *BMC Vet. Res.* **2020**, *16*, 1–8. [CrossRef] [PubMed]
62. Khodayar, M.J.; Kalantari, H.; Khorsandi, L.; Rashno, M.; Zeidooni, L. Upregulation of Nrf2- related cytoprotective genes expression by acetaminophen-induced acute hepatotoxicity in mice and the protective role of betaine. *Hum. Exp. Toxicol.* **2020**, 1–12. [CrossRef] [PubMed]
63. He, F.; Wu, C.; Li, P.; Li, N.; Zhang, D.; Zhu, Q.; Ren, W.; Peng, Y. Functions and signaling pathways of amino acids in intestinal inflammation. *Biomed. Res. Int.* **2018**, *2018*, 1–13. [CrossRef]
64. Han, H.; Yin, J.; Wang, B.; Huang, X.; Yao, J.; Zheng, J.; Fan, W.; Li, T.; Yin, Y. Effects of dietary lysine restriction on inflammatory responses in piglets. *Sci. Rep.* **2018**, *8*, 1–8. [CrossRef]
65. Wu, T.; Wang, C.; Ding, L.; Shen, Y.; Cui, H.; Wang, M.; Wang, H. Arginine relieves the inflammatory response and enhances the casein expression in bovine mammary epithelial cells induced by lipopolysaccharide. *Mediat. Inflamm.* **2016**, *2016*, 1–10. [CrossRef]
66. Hnia, K.; Gayraud, J.; Hugon, G.; Ramonatxo, M.; De La Porte, S.; Matecki, S.; Mornet, D. L-arginine decreases inflammation and modulates the nuclear factor-kappaB/matrix metalloproteinase cascade in mdx muscle fibers. *Am. J. Pathol.* **2008**, *172*, 1509–1519. [CrossRef]
67. Coburn, L.A.; Gong, X.; Singh, K.; Asim, M.; Scull, B.P.; Allaman, M.M.; Williams, C.S.; Rosen, M.J.; Washington, M.K.; Barry, D.P.; et al. L-arginine supplementation improves responses to injury and inflammation in dextran sulfate sodium colitis. *PLoS ONE* **2012**, *7*, e33546. [CrossRef]
68. Alamshah, A.; Spreckley, E.; Norton, M.; Kinsey-Jones, J.S.; Amin, A.; Ramgulam, A.; Cao, Y.; Johnson, R.; Saleh, K.; Akalestou, E.; et al. l-phenylalanine modulates gut hormone release and glucose tolerance, and suppresses food intake through the calcium-sensing receptor in rodents. *Int. J. Obes.* **2017**, *41*, 1693–1701. [CrossRef]
69. Oldenburger, A.; Roscioni, S.S.; Jansen, E.; Menzen, M.H.; Halayko, A.J.; Timens, W.; Meurs, H.; Maarsingh, H.; Schmidt, M. Anti-inflammatory role of the cAMP effectors Epac and PKA: Implications in chronic obstructive pulmonary disease. *PLoS ONE* **2012**, *7*, e31574. [CrossRef]
70. Liu, R.; Li, P.; Bi, W.C.; Ma, R.; Yin, Y.; Bi, K.; Li, Q. Plasma N-acetylputrescine, cadaverine and 1,3-diaminopropane: Potential biomarkers of lung cancer used to evaluate the ef cacy of anticancer drugs. *Oncotarget* **2017**, *8*, 88575–88585. [CrossRef]
71. Saxena, R.N.; Pendse, V.K.; Khanna, N.K. Anti-inflammatory and analgesic properties of four amino-acids. *Indian J. Physiol. Pharmacol.* **1984**, *28*, 299–305.
72. Kato, H.; Miura, K.; Nakano, S.; Suzuki, K.; Bannai, M.; Inoue, Y. Leucine-enriched essential amino acids attenuate inflammation in rat muscle and enhance muscle repair after eccentric contraction. *Amino Acids* **2016**, *48*, 2145–2155. [CrossRef] [PubMed]
73. Safer, D.; Brenes, M.; Dunipace, S.; Schad, S. Urocanic acid is a major chemoattractant for the skin-penetrating parasitic nematode Strongyloides stercoralis. *Proc. Natl. Acad. Sci. USA* **2007**, *104*, 1627–1630. [CrossRef]
74. Mastrofrancesco, A.; Ottaviani, M.; Aspite, N.; Cardinali, G.; Izzo, E.; Graupe, K.; Zouboulis, C.C.; Camera, E.; Picardo, M. Azelaic acid modulates the inflammatory response in normal human keratinocytes through PPARgamma activation. *Exp. Dermatol.* **2010**, *19*, 813–820. [CrossRef]
75. Andersen, F.A. Final report on the safety assessment of Maleic Acid. *Int. J. Toxicol.* **2007**, *26*, 125–130. [CrossRef]
76. Spreafico, A.; Millucci, L.; Ghezzi, L.; Geminiani, M.; Braconi, D.; Amato, L.; Chellini, F.; Frediani, B.; Moretti, E.; Collodel, G.; et al. Antioxidants inhibit SAA formation and pro-inflammatory cytokine release in a human cell model of alkaptonuria. *Rheumatology* **2013**, *52*, 1667–1673. [CrossRef]
77. Hegedus, Z.L.; Nayak, U. Homogentisic acid and structurally related compounds as intermediates in plasma soluble melanin formation and in tissue toxicities. *Arch. Int. Physiol. Biochim. Biophys.* **1994**, *102*, 175–181.
78. Darabi, Z.; Darand, M.; Yari, Z.; Hedayati, M.; Faghihi, A.; Agah, S.; Hekmatdoost, A. Inflammatory markers response to citrulline supplementation in patients with non-alcoholic fatty liver disease: A randomized, double blind, placebo-controlled, clinical trial. *BMC Res. Notes* **2019**, *12*, 1–5. [CrossRef]
79. Ham, D.J.; Gleeson, B.G.; Chee, A.; Baum, D.M.; Caldow, M.K.; Lynch, G.S.; Koopman, R. L-Citrulline protects skeletal muscle cells from cachectic stimuli through an iNOS-dependent mechanism. *PLoS ONE* **2015**, *10*, e0141572. [CrossRef]

80. Lee, Y.C.; Su, Y.T.; Liu, T.Y.; Tsai, C.M.; Chang, C.H.; Yu, H.R. L-arginine and L-citrulline supplementation have different programming effect on regulatory T-cells function of infantile rats. *Front. Immunol.* **2018**, *9*, 1–11. [CrossRef]
81. Faure, M.; Mettraux, C.; Moennoz, D.; Godin, J.-P.; Vuichoud, J.; Rochat, F.; Breuillé, D.; Obled, C.; Corthésy-Theulaz, I. Specific amino acids increase mucin synthesis and microbiota in dextran sulfate sodium–treated rats. *J. Nutr.* **2006**, *136*, 1558–1564. [CrossRef] [PubMed]
82. Ma, E.H.; Bantug, G.; Griss, T.; Condotta, S.; Johnson, R.M.; Samborska, B.; Mainolfi, N.; Suri, V.; Guak, H.; Balmer, M.L.; et al. Serine is an essential metabolite for effector T cell expansion. *Cell Metab.* **2017**, *25*, 345–357. [CrossRef]
83. Gaifem, J.; Goncalves, L.G.; Dinis-Oliveira, R.J.; Cunha, C.; Carvalho, A.; Torrado, E.; Rodrigues, F.; Saraiva, M.; Castro, A.G.; Silvestre, R. L-Threonine supplementation during Colitis onset delays disease recovery. *Front. Physiol.* **2018**, *9*, 1–7. [CrossRef]
84. Dong, Y.W.; Jiang, W.D.; Liu, Y.; Wu, P.; Jiang, J.; Kuang, S.Y.; Tang, L.; Tang, W.N.; Zhang, Y.A.; Zhou, X.Q.; et al. Threonine deficiency decreased intestinal immunity and aggravated inflammation associated with NF-kappaB and target of rapamycin signalling pathways in juvenile grass carp (Ctenopharyngodon idella) after infection with Aeromonas hydrophila. *Br. J. Nutr.* **2017**, *118*, 92–108. [CrossRef]
85. Mine, Y.; Zhang, H. Calcium-sensing receptor (CaSR)-mediated anti-inflammatory effects of L-amino acids in intestinal epithelial cells. *J. Agric. Food Chem.* **2015**, *63*, 9987–9995. [CrossRef]
86. Yue, Y.; Guo, Y.; Yang, Y. Effects of dietary L-tryptophan supplementation on intestinal response to chronic unpredictable stress in broilers. *Amino Acids* **2017**, *49*, 1227–1236. [CrossRef]
87. Islam, J.; Sato, S.; Watanabe, K.; Watanabe, T.; Ardiansyah; Hirahara, K.; Aoyama, Y.; Tomita, S.; Aso, H.; Komai, M.; et al. Dietary tryptophan alleviates dextran sodium sulfate-induced colitis through aryl hydrocarbon receptor in mice. *J. Nutr. Biochem.* **2017**, *42*, 43–50. [CrossRef]
88. Li, X.S.; Wang, Z.; Cajka, T.; Buffa, J.A.; Nemet, I.; Hurd, A.G.; Gu, X.; Skye, S.M.; Roberts, A.B.; Wu, Y.; et al. Untargeted metabolomics identifies trimethyllysine, a TMAO-producing nutrient precursor, as a predictor of incident cardiovascular disease risk. *JCI Insight* **2018**, *3*, 1–18. [CrossRef] [PubMed]
89. Lindsay, A.; Gieseg, S.P. Pterins as diagnostic markers of exercise-induced stress: A systematic review. *J. Sci. Med. Sport.* **2020**, *23*, 53–62. [CrossRef] [PubMed]
90. Pederzolli, C.D.; Mescka, C.P.; Zandona, B.R.; de Moura Coelho, D.; Sgaravatti, A.M.; Sgarbi, M.B.; de Souza Wyse, A.T.; Duval Wannmacher, C.M.; Wajner, M.; Vargas, C.R.; et al. Acute administration of 5-oxoproline induces oxidative damage to lipids and proteins and impairs antioxidant defenses in cerebral cortex and cerebellum of young rats. *Metab. Brain Dis.* **2010**, *25*, 145–154. [CrossRef]
91. Kalinowska, M.; Mazur, L.; Jabłońska-Trypuć, A.; Lewandowski, W. A new calcium 2,5-dihydroxybenzoate: Synthesis, characterization and antioxidant studies and stress mediated cytotoxity in MCF-7 cells. *J. Saudi Chem. Soc.* **2018**, *22*, 742–756. [CrossRef]
92. Pearson, M.S.; Tribolet, L.; Cantacessi, C.; Periago, M.V.; Valero, M.A.; Jariwala, A.R.; Hotez, P.; Diemert, D.; Loukas, A.; Bethony, J. Molecular mechanisms of hookworm disease: Stealth, virulence, and vaccines. *J. Allergy Clin. Immunol.* **2012**, *130*, 13–21. [CrossRef]
93. Rochat, B. Proposed confidence scale and ID score in the identification of known-unknown compounds using high resolution MS data. *J. Am. Soc. Mass Spectrom.* **2017**, *28*, 709–723. [CrossRef]
94. Gika, H.G.; Theodoridis, G.A.; Plumb, R.S.; Wilson, I.D. Current practice of liquid chromatography-mass spectrometry in metabolomics and metabonomics. *J. Pharm. Biomed. Anal.* **2014**, *87*, 12–25. [CrossRef]
95. Cajka, T.; Vaclavikova, M.; Dzuman, Z.; Vaclavik, L.; Ovesna, J.; Hajslova, J. Rapid LC-MS-based metabolomics method to study the Fusarium infection of barley. *J. Sep. Sci.* **2014**, *37*, 912–919. [CrossRef]
96. Barrett, J. Developmental aspects of metabolism in parasites. *Int. J. Parasitol.* **1987**, *17*, 105–110. [CrossRef]
97. Bennuru, S.; Lustigman, S.; Abraham, D.; Nutman, T.B. Metabolite profiling of infection-associated metabolic markers of onchocerciasis. *Mol. Biochem. Parasitol.* **2017**, *215*, 58–69. [CrossRef]
98. Ryan, S.M.; Eichenberger, R.M.; Ruscher, R.; Giacomin, P.R.; Loukas, A. Harnessing helminth-driven immunoregulation in the search for novel therapeutic modalities. *PLoS Pathog.* **2020**, *16*, e1008508. [CrossRef] [PubMed]
99. Craig, S.A.S. Betaine in human nutrition. *Am. J. Clin. Nutr.* **2004**, *80*, 539–549. [CrossRef]

100. Saric, J.; Li, J.V.; Utzinger, J.; Wang, Y.; Keiser, J.; Dirnhofer, S.; Beckonert, O.; Sharabiani, M.T.; Fonville, J.M.; Nicholson, J.K.; et al. Systems parasitology: Effects of Fasciola hepatica on the neurochemical profile in the rat brain. *Mol. Syst. Biol.* **2010**, *6*, 1–10. [CrossRef]
101. Beis, I.; Barrett, J. Energy metabolism in developing Ascaris lumbricoides eggs II. The steady state content of intermediary metabolites. *Dev. Biol.* **1975**, *42*, 188–195. [CrossRef]
102. Wangchuk, P.; Shepherd, C.; Constantinoiu, C.; Ryan, R.Y.M.; Kouremenos, K.A.; Becker, L.; Jones, L.; Buitrago, G.; Giacomin, P.; Wilson, D.; et al. Hookworm-derived metabolites suppress pathology in a mouse model of colitis and inhibit secretion of key inflammatory cytokines in primary human leukocytes. *Infect. Immun.* **2019**, *87*, 1–19. [CrossRef] [PubMed]
103. Emmett, M. Acetaminophen toxicity and 5-oxoproline (pyroglutamic acid): A tale of two cycles, one an ATP-depleting futile cycle and the other a useful cycle. *Clin. J. Am. Soc. Nephrol.* **2014**, *9*, 191–200. [CrossRef]
104. Liss, D.B.; Paden, M.S.; Schwarz, E.S.; Mullins, M.E. What is the clinical significance of 5-oxoproline (pyroglutamic acid) in high anion gap metabolic acidosis following paracetamol (acetaminophen) exposure? *Clin. Toxicol.* **2013**, *51*, 817–827. [CrossRef] [PubMed]
105. Loffler, M.; Carrey, E.A.; Zameitat, E. Orotate (orotic acid): An essential and versatile molecule. *Nucleos. Nucleot. Nucl.* **2016**, *35*, 566–577. [CrossRef]
106. Hill, B.; Kilsby, J.; Rogerson, G.W.; Mcintosh, R.T.; Ginger, C.D. The enzymes of pyrimidine biosynthesis in a range of parasitic protozoa and helminths. *Mol. Biochem. Parasitol.* **1981**, *2*, 123–134. [CrossRef]
107. Longo, N. Disorders of biopterin metabolism. *J. Inherit. Metab. Dis.* **2009**, *32*, 333–342. [CrossRef] [PubMed]
108. Arias-Barrau, E.; Olivera, E.R.; Luengo, J.M.; Fernandez, C.; Galan, B.; Garcia, J.L.; Diaz, E.; Minambres, B. The homogentisate pathway: A central catabolic pathway involved in the degradation of L-phenylalanine, L-tyrosine, and 3-hydroxyphenylacetate in Pseudomonas putida. *J. Bacteriol.* **2004**, *186*, 5062–5077. [CrossRef]
109. Sterkel, M.; Perdomo, H.D.; Guizzo, M.G.; Barletta, A.B.; Nunes, R.D.; Dias, F.A.; Sorgine, M.H.; Oliveira, P.L. Tyrosine detoxification is an essential trait in the life history of blood-feeding arthropods. *Curr. Biol.* **2016**, *26*, 2188–2193. [CrossRef] [PubMed]
110. Wang, S.L.; Li, H.T.; Zhang, L.J.; Lin, Z.H.; Kuo, Y.H. Conversion of squid pen to homogentisic acid via Paenibacillus sp. TKU036 and the antioxidant and anti-inflammatory activities of homogentisic acid. *Mar. Drugs* **2016**, *14*, 183. [CrossRef]
111. Allen, J.E.; MacDonald, A.S. Profound suppression of cellular proliferation mediated by the secretions of nematodes. *Parasite Immunol.* **1998**, *20*, 241–247. [CrossRef]
112. Porth, C. *Essentials of Pathophysiology: Concepts of Altered Health States*; Lippincott Williams & Wilkins: Philadelphia, PA, USA, 2011; pp. 1–1248.
113. Peachey, L.E.; Castro, C.; Molena, R.A.; Jenkins, T.P.; Griffin, J.L.; Cantacessi, C. Dysbiosis associated with acute helminth infections in herbivorous youngstock - observations and implications. *Sci. Rep.* **2019**, *9*, 1–16. [CrossRef]
114. Fotiadis, C.; Adamis, S.; Misiakos, E.P.; Genetzakis, M.; Antonakis, P.T.; Tsekouras, D.K.; Gorgoulis, V.G.; Zografos, G.C.; Papalois, A.; Fotinou, M.; et al. The prophylactic effect of L-arginine in acute ischaemic Colitis in a rat model of ischaemia/reperfusion injury. *Acta Chir. Belg.* **2016**, *107*, 192–200. [CrossRef]
115. Zhu, H.L.; Liu, Y.L.; Xie, X.L.; Huang, J.J.; Hou, Y.Q. Effect of L-arginine on intestinal mucosal immune barrier function in weaned pigs after Escherichia coli LPS challenge. *Innate Immun.* **2013**, *19*, 242–252. [CrossRef]
116. Sato, S.; Hirayama, T.; Hirazawa, N. Lipid content and fatty acid composition of the monogenean Neobenedenia girellae and comparison between the parasite and host fish species. *Parasitology* **2008**, *135*, 967–975. [CrossRef]
117. Zeng, C.; Wen, B.; Hou, G.; Lei, L.; Mei, Z.; Jia, X.; Chen, X.; Zhu, W.; Li, J.; Kuang, Y.; et al. Lipidomics profiling reveals the role of glycerophospholipid metabolism in psoriasis. *Gigascience* **2017**, *6*, 1–11. [CrossRef]
118. Ward, P.F. Aspects of helminth metabolism. *Parasitology* **1982**, *84*, 177–194. [CrossRef]
119. Wang, T.; Nie, S.; Ma, G.; Korhonen, P.K.; Koehler, A.V.; Ang, C.S.; Reid, G.E.; Williamson, N.A.; Gasser, R.B. The developmental lipidome of Haemonchus contortus. *Int. J. Parasitol.* **2018**, *48*, 887–895. [CrossRef] [PubMed]
120. Henry, P.; Owopetu, O.; Adisa, D.; Nguyen, T.; Anthony, K.; Ijoni-Animadu, D.; Jamadar, S.; Abdel-Rahman, F.; Saleh, M.A. Fatty acids composition of Caenorhabditis elegans using accurate mass GCMS-QTOF. *J. Environ. Sci. Health B* **2016**, *51*, 546–552. [CrossRef]
121. Sinensky, M. Homeoviscous adaptation—A homeostatic process that regulates the viscosity of membrane lipids in *Escherichia Coli*. *Proc. Natl. Acad. Sci. USA* **1974**, *71*, 522–525. [CrossRef]

122. Ma, D.K.; Li, Z.; Lu, A.Y.; Sun, F.; Chen, S.; Rothe, M.; Menzel, R.; Sun, F.; Horvitz, H.R. Acyl-CoA Dehydrogenase Drives Heat Adaptation by Sequestering Fatty Acids. *Cell* **2015**, *161*, 1152–1163. [CrossRef]
123. Mangmee, S.; Adisakwattana, P.; Tipthara, P.; Simanon, N.; Sonthayanon, P.; Reamtong, O. Lipid profile of Trichinella papuae muscle-stage larvae. *Sci. Rep.* **2020**, *10*, 10125. [CrossRef]
124. Wewer, V.; Makepeace, B.L.; Tanya, V.N.; Peisker, H.; Pfarr, K.; Hoerauf, A.; Dormann, P. Lipid profiling of the filarial nematodes Onchocerca volvulus, Onchocerca ochengi and Litomosoides sigmodontis reveals the accumulation of nematode-specific ether phospholipids in the host. *Int. J. Parasitol.* **2017**, *47*, 903–912. [CrossRef]
125. Lee, D.L. Changes in adult Nippostrongylus brasiliensis during the development of immunity to this nematode in rats. 2. Total lipids and neutral lipids. *Parasitology* **1971**, *63*, 271–274. [CrossRef]
126. Barrett, J. *Biochemistry of Parasitic Helminths*; MacMillan Publishers Ltd.: New York, NY, USA, 1981.
127. Welty, F.K. How do elevated triglycerides and low HDL-cholesterol affect inflammation and atherothrombosis? *Curr. Cardiol. Rep.* **2013**, *15*, 1–13. [CrossRef]
128. Wang, X.; Devaiah, S.P.; Zhang, W.; Welti, R. Signaling functions of phosphatidic acid. *Prog. Lipid Res.* **2006**, *45*, 250–278. [CrossRef] [PubMed]
129. Zhang, F.; Wang, Z.; Lu, M.; Yonekubo, Y.; Liang, X.; Zhang, Y.; Wu, P.; Zhou, Y.; Grinstein, S.; Hancock, J.F.; et al. Temporal production of the signaling lipid phosphatidic acid by phospholipase D2 determines the output of extracellular signal-regulated kinase signaling in cancer cells. *Mol. Cell Biol.* **2014**, *34*, 84–95. [CrossRef]
130. Modha, J.; Roberts, M.C.; Robertson, W.M.; Sweetman, G.; Powell, K.A.; Kennedy, M.W.; Kusel, J.R. The surface coat of infective larvae of Trichinella spiralis. *Parasitology* **1999**, *118*, 509–522. [CrossRef] [PubMed]
131. Nervi, F. Significance of biliary phospholipids for maintenance of the gastrointestinal mucosal barrier and hepatocellular integrity. *Gastroenterology* **2000**, *118*, 1265–1267. [CrossRef]
132. Stremmel, W.; Merle, U.; Zahn, A.; Autschbach, F.; Hinz, U.; Ehehalt, R. Retarded release phosphatidylcholine benefits patients with chronic active ulcerative colitis. *Gut* **2005**, *54*, 966–971. [CrossRef]
133. Treede, I.; Braun, A.; Sparla, R.; Kuhnel, M.; Giese, T.; Turner, J.R.; Anes, E.; Kulaksiz, H.; Fullekrug, J.; Stremmel, W.; et al. Anti-inflammatory effects of phosphatidylcholine. *J. Biol. Chem.* **2007**, *282*, 27155–27164. [CrossRef] [PubMed]
134. Camberis, M.; Le Gros, G.; Urban, J.J. Animal model of Nippostrongylus brasiliensis and Heligmosomoides polygyrus. *Curr. Protoc. Immunol.* **2003**, *55*, 19.12.11–19.12.27.
135. Creek, D.J.; Chua, H.H.; Cobbold, S.A.; Nijagal, B.; MacRae, J.I.; Dickerman, B.K.; Gilson, P.R.; Ralph, S.A.; McConville, M.J. Metabolomics-based screening of the malaria box reveals both novel and established mechanisms of action. *Antimicrob. Agents Chemother.* **2016**, *60*, 6650–6663. [CrossRef]
136. Aurelio, L.; Scullino, C.V.; Pitman, M.R.; Sexton, A.; Oliver, V.; Davies, L.; Rebello, R.J.; Furic, L.; Creek, D.J.; Pitson, S.M.; et al. From sphingosine kinase to dihydroceramide desaturase: A structure-activity relationship (SAR) study of the enzyme inhibitory and anticancer activity of 4-((4-(4-chlorophenyl)thiazol-2-yl)amino)phenol (SKI-II). *J. Med. Chem.* **2016**, *59*, 965–984. [CrossRef] [PubMed]
137. Creek, D.J.; Jankevics, A.; Burgess, K.E.; Breitling, R.; Barrett, M.P. IDEOM: An Excel interface for analysis of LC-MS-based metabolomics data. *Bioinformatics* **2012**, *28*, 1048–1049. [CrossRef]
138. Scheltema, R.A.; Jankevics, A.; Jansen, R.C.; Swertz, M.A.; Breitling, R. PeakML/mzMatch: A file format, Java library, R library, and tool-chain for mass spectrometry data analysis. *Anal. Chem.* **2011**, *83*, 2786–2793. [CrossRef]
139. Chong, J.; Soufan, O.; Li, C.; Caraus, I.; Li, S.; Bourque, G.; Wishart, D.S.; Xia, J. MetaboAnalyst 4.0: Towards more transparent and integrative metabolomics analysis. *Nucleic Acids Res.* **2018**, *46*, W486–W494. [CrossRef] [PubMed]

Publisher's Note: MDPI stays neutral with regard to jurisdictional claims in published maps and institutional affiliations.

© 2020 by the authors. Licensee MDPI, Basel, Switzerland. This article is an open access article distributed under the terms and conditions of the Creative Commons Attribution (CC BY) license (http://creativecommons.org/licenses/by/4.0/).